ARTICLE

Eph signaling controls mitotic spindle orientation and cell proliferation in neuroepithelial cells

Maribel Franco and Ana Carmena

Mitotic spindle orientation must be tightly regulated during development and adult tissue homeostasis. It determines cell-fate specification and tissue architecture during asymmetric and symmetric cell division, respectively. Here, we uncover a novel role for Ephrin–Eph intercellular signaling in controlling mitotic spindle alignment in *Drosophila* optic lobe neuroepithelial cells through aPKC activity–dependent myosin II regulation. We show that conserved core components of the mitotic spindle orientation machinery, including Discs Large1, Mud/NuMA, and Canoe/Afadin, mislocalize in dividing *Eph* mutant neuroepithelial cells and produce spindle alignment defects in these cells when they are down-regulated. In addition, the loss of Eph leads to a Rho signaling–dependent activation of the PI3K–Akt1 pathway, enhancing cell proliferation within this neuroepithelium. Hence, Eph signaling is a novel extrinsic mechanism that regulates both spindle orientation and cell proliferation in the *Drosophila* optic lobe neuroepithelium. Similar mechanisms could operate in other *Drosophila* and vertebrate epithelia.

Introduction

A precise regulation of mitotic spindle orientation is crucial during development and adult tissue homeostasis. It determines cell fate specification and tissue architecture in the context of asymmetric and symmetric cell division, respectively (Morin and Bellaïche, 2011; Lu and Johnston, 2013; Williams and Fuchs, 2013). The positioning of the spindle during cell division involves autonomous and nonautonomous mechanisms. However, while the intrinsic factors that control spindle orientation have been extensively studied over the past decades, our knowledge about the extrinsic signals that modulate this process and their link with the intrinsic spindle orientation machinery remains limited (Werts and Goldstein, 2011; Williams and Fuchs, 2013).

Regarding the autonomous mechanisms, intrinsic polarity cues linked to the cell cortex converge on astral microtubule-associated motor complexes, these exerting the pulling forces that orientate the spindle (Williams and Fuchs, 2013). The core components of the spindle orientation machinery are few and well conserved, differing slightly depending on the cell type and the mode of cell division (Morin and Bellaïche, 2011). For example, in asymmetrically dividing *Drosophila melanogaster* neuroblasts (NBs), the apical proteins Par-6, Par-3 (Bazooka, Baz, in *Drosophila*), and atypical PKC (aPKC) associate with Inscuteable (Insc). The Par-Insc complex recruits Partner of Insc (Pins)/LGN to the apical pole, where it binds the Gαi subunit anchored to the membrane, orchestrating the orientation of the spindle along the apico–basal axis of cell polarity (Lu and Johnston, 2013). This process requires the PDZ protein Canoe (Cno)/Afadin, which after being phosphorylated by the Warts/LATS1-2 kinase, binds to the Pins/LGN^{TPRs} domain and displaces Insc bound to the same region (Yu et al., 2000; Wee et al., 2011; Keder et al., 2015). Cno/Afadin then facilitates the recruitment of Discs Large1 (Dlg1; Keder et al., 2015) to the Pins/LGN^{Linker} domain (Johnston et al., 2009) and of Mushroom body defect (Mud)/NuMA, which also binds to the Pins/LGN^{TPRs} domain, displacing Cno/Afadin (Bowman et al., 2006; Izumi et al., 2006; Siller et al., 2006; Speicher et al., 2008; Keder et al., 2015). In turn, Dlg1 and Mud/NuMA associate with Khc-73 and the Dynein–Dynactin complex, respectively, which bind to astral microtubules anchoring the spindle and promoting the pulling forces required for its correct orientation (Johnston et al., 2009). In symmetrically dividing epithelial cells, the spindle is oriented parallel to the plane of the tissue (planar division). In this process, the intrinsic regulators Pins/LGN, Gαi, and the Mud/NuMA–Dynein complex are also found at the core of the spindle orientation machinery (Morin and Bellaïche, 2011; Bergstralh et al., 2013a). However, it was recently shown that Pins/LGN is not required for the planar orientation of the spindle in epithelial cells of *Drosophila* wing discs, and that only the Mud/NuMA–Dynein–Dynactin complex is critical for this process (Bergstralh et al., 2016).

Developmental Neurobiology Department, Instituto de Neurociencias, Consejo Superior de Investigaciones Científicas/Universidad Miguel Hernández, Alicante, Spain.

Correspondence to Ana Carmena: acarmena@umh.es.

Regarding the nonautonomous mechanisms, extrinsic mechanical cues have long been implicated in coordinating spindle orientation (Hertwig, 1884; Morin and Bellaïche, 2011; Nestor-Bergmann et al., 2014). In this context, the actomyosin network is an important link between the external forces and mitotic spindle positioning (Severson and Bowerman, 2003; Goulding et al., 2007). The Wnt-activated planar cell polarity pathway has been widely implicated in spindle orientation in different systems (Gong et al., 2004; Saburi et al., 2008; Castanon and González-Gaitán, 2011). This pathway impinges directly on the spindle orientation machinery by interacting with the conserved intrinsic spindle regulator Mud/NuMA, in both *Drosophila* and zebrafish (Ségalen et al., 2010). Other extrinsic cues also affect spindle orientation in vertebrates, such as Cadherin-mediated intercellular signaling or the FGF/Ras/ERK signaling pathway, although the downstream mechanisms that directly link them to the spindle orientation machinery are poorly understood (den Elzen et al., 2009; Castanon and González-Gaitán, 2011; Tang et al., 2011; Žigman et al., 2011). In this regard, a direct interaction between E-cadherin and LGN (Pins in *Drosophila*) has recently been identified in cultured cells (Gloerich et al., 2017). Likewise, a few years ago Semaphorin-Plexin signaling was identified as a novel extrinsic regulator of spindle orientation during kidney development and repair, as well as in the mouse spinal cord. This signaling controls the activity of Cdc42, a known regulator of spindle alignment (Arbeille et al., 2015; Xia et al., 2015).

Like Semaphorin-Plexin, there has been much interest in the role of Ephrin–Eph signaling during axon guidance (Cramer and Miko, 2016; Kania and Klein, 2016). However, this pathway also regulates different developmental processes, as well as adult tissue homeostasis and carcinogenesis (Batlle and Wilkinson, 2012; Lisabeth et al., 2013; Wilkinson, 2014; Jungas et al., 2016; Kania and Klein, 2016). A large family of ~14 Eph receptors and 8 Ephrin ligands has been identified in vertebrates, whereas *Drosophila* has only 1 Eph receptor and 1 Ephrin ligand (Scully et al., 1999; Bossing and Brand, 2002). Both Eph tyrosine kinase receptors and their Ephrin ligands are membrane-bound proteins triggering cell–cell contact–mediated signaling, either through the receptor (forward signaling) or the ligand (reverse signaling; Lisabeth et al., 2013; Kania and Klein, 2016). This reverse signaling through the Ephrin intracellular domain can affect cell junctions, cell–cell adhesion, and ultimately tissue architecture (Jones et al., 1998; Chong et al., 2000; Lee et al., 2008; Lee and Daar, 2009; Arvanitis et al., 2013). Ephrin reverse signaling has also been shown to regulate the balance between proliferation and differentiation in the neural progenitor cells of the mammalian cerebral cortex, favoring the maintenance of the progenitors in detriment to their differentiation (Qiu et al., 2008). Ephrin B1–dependent forward EphA4 signaling has also been implicated in promoting progenitor proliferation in the developing cerebral cortex (North et al., 2009). However, a role for EphA receptors in inducing the differentiation of mammalian neural progenitor cells in vitro and in vivo has also been proposed (Aoki et al., 2004; Laussu et al., 2014).

Here, we uncover a novel function for Ephrin–Eph intercellular signaling as a new extrinsic cue controlling mitotic spindle orientation in the symmetrically dividing neuroepithelial cells in the *Drosophila* optic lobe. This function relies on aPKC activity–dependent myosin II regulation, which influences the architecture of the neuroepithelium (NE) and the cortical distribution of core components of the spindle orientation machinery. In addition, we identify a requirement for Ephrin–Eph signaling to regulate proliferation in this NE through the Rho signaling–dependent inhibition of the phosphoinositide-3-kinase (PI3K)–Akt pathway.

Results

Eph signaling is required to maintain a correct NE architecture

Having initially detected a widespread, punctate distribution of the Eph receptor in the *Drosophila* optic lobe NE (Fig. 1, A and B; and Fig. S1), we were interested to analyze a potential function of Eph signaling in the development of this tissue. Given that polarity is an intrinsic characteristic of epithelial cells, we started by analyzing the distribution of well-conserved epithelial polarity cues in the optic lobe NE of Eph^{x652}-null homozygote mutants at the late third instar larval (L3) stage. Specifically, we tested the apical marker Patj; the markers of the subapical region (equivalent to the tight junction region in vertebrates) Par-6 and aPKC; adherens junctions (AJs) proteins such as E-cadherin (Shotgun, Shg, in *Drosophila*), Par-3 (Baz in *Drosophila*), and Cno/Afadin; the basolateral proteins Dlg1 and Scribble (Scrib); and Myospheroid (Mys), the β subunit of the integrin dimer that accumulates in the basal domain of epithelial cells (Fig. 1, C–Q). Significantly, we detected an anomalous apical enrichment of Dlg1 in the neuroepithelial cells of Eph^{x652} mutants (Fig. 1, C–D′), while the general apico-basal distribution of the rest of the proteins tested did not appear to be altered. Nevertheless, the local distribution and thresholds of these proteins revealed a disturbed NE architecture. For example, less Shg/E-cadherin and Cno/Afadin accumulated at AJs in Eph^{x652} mutants (Fig. 1, K, K″, L, and L″–N), and the apical localization of Patj and aPKC, as well as the basal distribution of Mys/β integrin subunit, were less uniform than in control neuroepithelia (Fig. 1, E–H′ and O–P′). An apical disruption of the NE in Eph^{x652} mutants was also very apparent in some cases (Fig. 1, I–J′ and K–L″). Similar phenotypes, or milder in the case of Dlg1 apical expansion, were observed in other *Eph* mutants, such as a kinase dead mutant, as well as following $Ephrin^{RNAi}$ down-regulation (Fig. S2). We also noticed that while the cell nuclei lie at different positions in control neuroepithelia, in a pseudostratified organization, at this late L3 stage the cell nuclei tended to align at the same level in Eph^{x652} neuroepithelia (simple organization). Consequently, mutant neuroepithelia generally looked narrower than those of controls (Fig. 1, R–T). Hence, Eph signaling is necessary to maintain the correct architecture of the NE.

Eph signaling is required for the correct distribution of actomyosin and for subapical region formation in neuroepithelial cells

Given that the cortical distribution of actomyosin helps model cell shape and size, we assessed the distribution of both actin and the regulatory light chain of the nonmuscle myosin II (Spaghetti
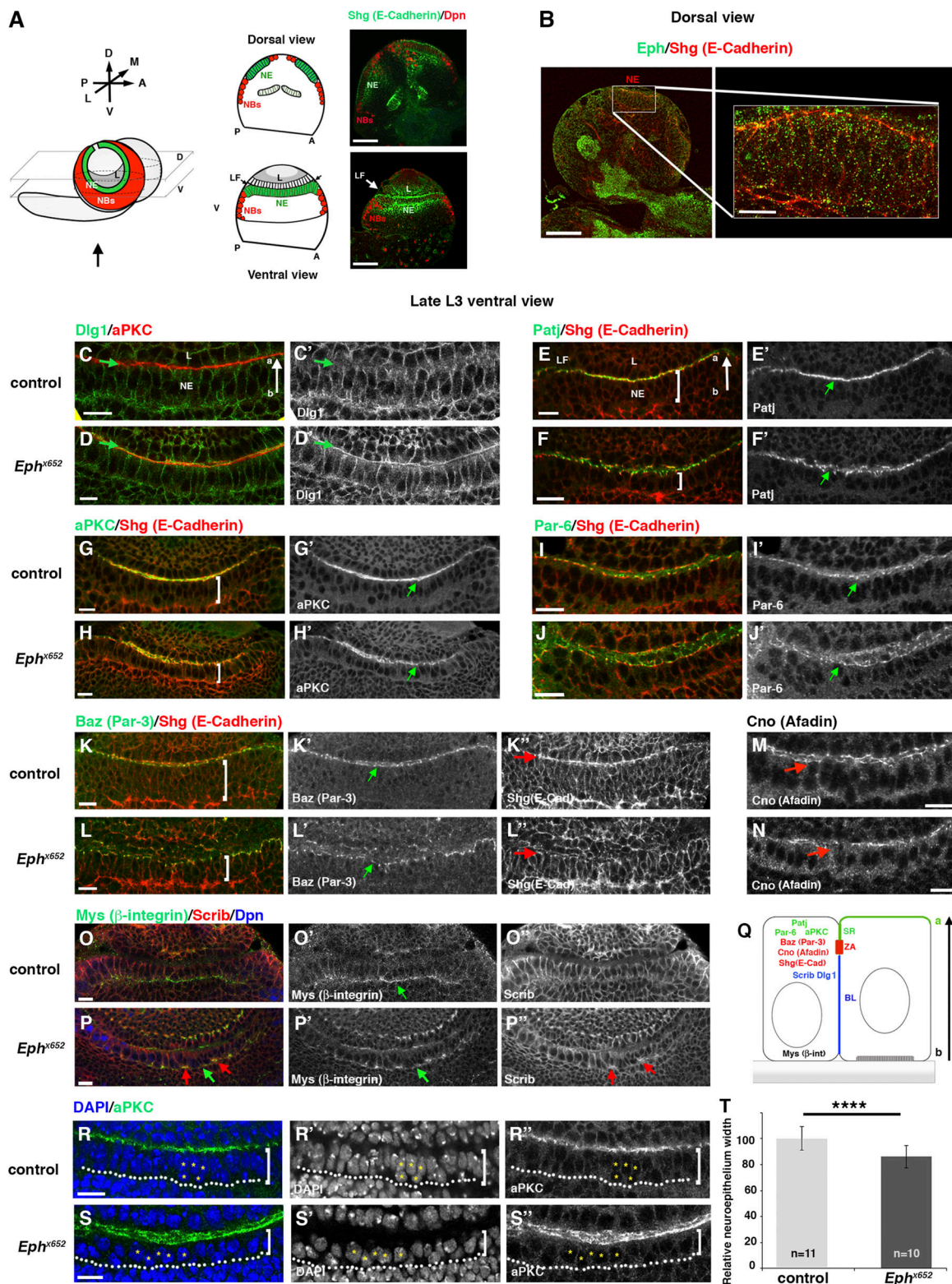
Figure 1. **Eph signaling is required to maintain a correct NE architecture. (A)** Diagram of the *Drosophila* larval central nervous system composed of the ventral cord and two brain hemispheres. The optic lobe NE from one brain hemisphere is shown in green and the medial NBs in red (A, anterior; P, posterior; M, medial; L, lateral; D, dorsal; V, ventral). A detail of a dorsal and a ventral view is shown on the right (L, lamina; LF, lamina furrow). **(B)** Expression of Eph (green) in the optic lobe NE labeled with Shg (E-cadherin, in red). The inset shows a detail of the NE with a punctate Eph expression associated with cell membranes (see also Fig. S1). **(C–P")** Apico-basal distribution of different polarity cues in control and *Eph^{x652}* mutant neuroepithelia. The basolateral protein Dlg1 expands apically in the *Eph^{x652}* mutant NE (green arrows in C–D'), while the apico-basal localization of other proteins remains unaffected, although their thresholds and local distribution are altered (green and red arrows; see also text). The brackets indicate the width of the NE; a, apical; b, basal. **(Q)** Schematic representation of two neuroepithelial cells showing the regions that define the cell polarity and some representative proteins in each of these zones (a, apical; SR, subapical

region; ZA, zonula adherens or AJs; BL, basolateral; b, basal). **(R–T)** Control neuroepithelia show a pseudostratified organization due to the arrangement of cell nuclei at different positions along the apico-basal cell axis (asterisks in R–R"). In Eph^{x652} mutant neuroepithelia, cell nuclei align at the same level (asterisks in S–S"); the dotted line indicates the basal part of the NE. **(T)** Quantification of the width of the Eph^{x652} NE ($n = 10$) relative to the control ($n = 11$). The data were analyzed with an unpaired two-tailed Student's t test; ****, $P < 0.0001$; error bars indicate the SD. Scale bars, 50 µm in A and B and 10 µm in the rest of the panels (including the inset in B).

squash [Sqh] in *Drosophila*) in *Eph* neuroepithelia. At the early L3 stage, the distribution of both actin and myosin II (Sqh) was already compromised in *Eph* mutants, at least in part explaining the defects in the architecture of the NE detected at late L3 on this mutant background (Fig. 2, A–B"). Intriguingly, we observed that the subapical region, well defined between the AJs and the most apical cell region in control neuroepithelial cells, was collapsed in *Eph* mutant neuroepithelia, and Shg (E-cadherin)⁺ AJs were in close contact or intermingled with the apical region (Fig. 2, A–B"). In addition, aPKC, normally localized to the subapical region, was completely apical in *Eph* mutant neuroepithelia (Fig. 2, C–D"). Finally, to determine the involvement of myosin II (Sqh) in these *Eph* mutant phenotypes, we looked at a phosphomutant form of Sqh (Sqh^{A20A2I}, hereafter Sqh^{AA}; Jordan and Karess, 1997) at the early L3 stage. Again, some disruption of the subapical region was detected in neuroepithelial cells, although aPKC in *myosin II* mutant (Sqh^{AA}) neuroepithelia was not so apically expanded as in *Eph* mutants (Fig. 2, E–E"). From these observations, we conclude that Eph signaling is required to establish the correct optic lobe NE architecture, at least partially through myosin II regulation.

Eph controls mitotic spindle orientation and interkinetic nuclear migration (INM) in optic lobe neuroepithelial cells

An intact actomyosin cell cortex is emerging as an important requirement for a correct mitotic spindle orientation

(Luxenburg et al., 2011; Nakajima et al., 2013; Zheng et al., 2013; Lancaster and Baum, 2014; di Pietro et al., 2016). Given that we found alterations in both the actin and myosin II (Sqh) distribution in *Eph* optic lobe neuroepithelia (Fig. 2, A–B"), we analyzed the mitotic spindle orientation in *Eph* mutants. We performed this analysis at the early L3 stage, a moment at which cells divide parallel to the plane of the NE in WT optic lobes (Rujano et al., 2013). While in control neuroepithelia most spindles were positioned in parallel (0°–30° angle), in Eph^{x652} homozygotes most of them were oriented perpendicular or at an oblique angle (>30°) to the plane of the NE (Fig. 3, A and B). Similar phenotypes to that of Eph^{x652} mutants were found in neuroepithelia specifically expressing either Eph^{RNAi} or $Ephrin^{RNAi}$, as well as in Eph^{KD} (kinase dead) mutant neuroepithelia (Fig. 3, C–E). We also observed defects in the position of the nucleus in neuroepithelial cells during mitosis at this early L3 stage. As mentioned above, WT optic lobe neuroepithelial cells arrange their nuclei at different positions along the apico–basal axis. This is due to the INM (Kosodo, 2012; Rujano et al., 2013) that shifts cells closer to the apical surface to divide (Rujano et al., 2013; Fig. 3 F). In early L3 *Eph* and $Ephrin^{RNAi}$ mutants, we observed mitotic cells at random positions along the apico–basal cell axis (Fig. 3, B, C, E, G, and H). Spindle orientation failed more often in mitotic cells at basal positions than at apical positions in Eph^{x652} mutant neuroepithelia, while in controls there was a similar percentage of defects in apical and basal cells
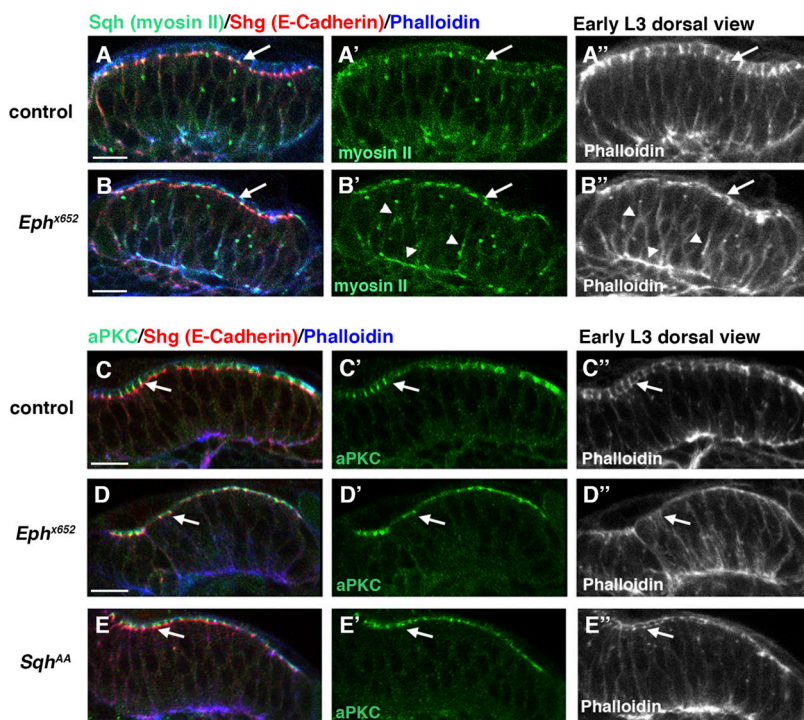
Figure 2. **Eph signaling is required for the correct distribution of actomyosin and for subapical region formation in neuroepithelial cells. (A–D")** Myosin II (Sqh) and actin (Phalloidin) show an altered distribution in Eph^{x652} mutant neuroepithelia (arrowheads in B' and B") relative to the control (A–A"). The subapical region is well defined in control neuroepithelia (arrow in A–A") yet it is collapsed in Eph^{x652} mutant neuroepithelia (arrow in B–B"), in which the subapical protein aPKC is intermingled with the AJs protein E-cadherin (Shg; arrow in D–D"; compare with C–C"). **(E–E")** A myosin II (Sqh) mutant NE showing the collapse of the subapical region (arrow), which is less extreme than in Eph^{x652} mutant neuroepithelia. Scale bars, 10 µm.
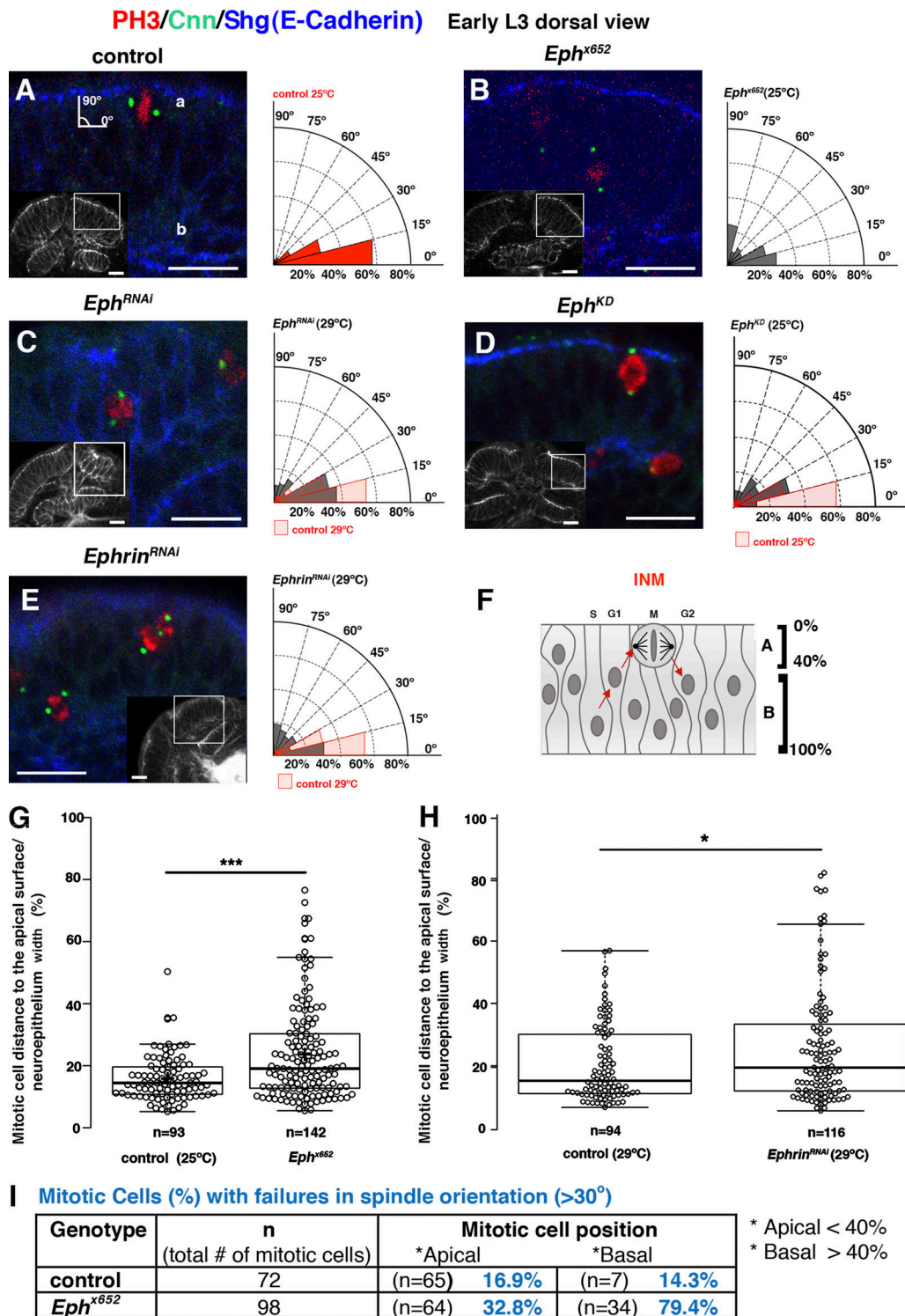
Figure 3. **Eph controls mitotic spindle orientation and INM in optic lobe neuroepithelial cells. (A–E)** Control early L3 stage mitotic neuroepithelial cells (n = 72 at 25°C and n = 75 at 29°C) show mostly parallel divisions (0–30°), while *Eph* and *Ephrin* mutants show a significant number of perpendicular or oblique divisions (>30°); n = 98, P < 0.0001 in B; n = 56, P < 0.05 in C; n = 38, P < 0.0001 in D; and n = 78, P < 0.0001 in E. A χ^2 test was used to compare the control and mutant values. The insets in each panel show the optic lobe NE from one brain hemisphere in black and white, highlighting the region (rectangle/square) in which mitoses were found (shown in the whole color panel). The Gal4 line c855 was used to express *Eph^RNAi* and *Ephrin^RNAi* in the NE. **(F–H)** Neuroepithelial cell nuclei lie at different positions along the apico-basal cell axis depending on the stage of the cell cycle, a phenomenon known as INM. Mitoses (M) occur at the most apical part of control neuroepithelia (F), while they are randomly distributed along the apico-basal cell axis in the *Eph^x652* and *Ephrin^RNAi* mutants (G and H). The data were analyzed with a Mann–Whitney U test, with the central lines showing the median and the limits of the box indicating the lower and upper quartiles determined by R software; ***, P < 0.001 and *, P < 0.05. **(I)** The mitotic cells located basally in the *Eph^x652* mutant NE (>40% of the NE width, see F) show a much higher percentage of spindle orientation defects (>30°) than control mitotic basal cells. Scale bars, 10 µm.

Franco and Carmena

(Fig. 3 I). This result suggests that the basal position of mitotic cells contributes to the effects on spindle orientation failures in *Eph^x652* mutants. However, mitotic cell position is not the only driver of the phenotype observed, as correctly located apical cells in mutant neuroepithelia still showed a higher proportion of spindle defects than control apical cells (Fig. 3 I). Thus, Eph regulates mitotic spindle orientation and INM in the optic lobe NE.

Eph controls spindle orientation by regulating myosin II

To examine how Eph regulates the orientation of the mitotic spindle and given the altered myosin II distribution in *Eph* mutant neuroepithelial cells (Fig. 2), we first analyzed the phenotype of the phosphomutant form of myosin II (*Sqh^AA*; Jordan and Karess, 1997), identifying mitotic spindle alterations in the optic lobe neuroepithelial cells similar to those found in *Eph* mutants (Fig. 4 A). In mammals, both Eph receptors and ephrin ligands can activate the RhoA small GTPase, which in turn induces the activity of its downstream effector RhoA-associated kinase (ROCK; Wahl et al., 2000; Noren and Pasquale, 2004; Lisabeth et al., 2013). Activated ROCKs phosphorylate the myosin II light chain in both mammals and *Drosophila*, inducing myosin–actin interactions and therefore myosin ATPase activity (Amano et al., 1996; Winter et al., 2001; Fig. 4 B). The myosin II (Sqh) defects we observed in *Eph* mutant neuroepithelia at the early L3 stage (Fig. 2, A–B″) were maintained at late L3 (Fig. 4, C–D‴). Hence, we assessed whether Eph acts through a ROCK to regulate myosin II (Sqh) in our system, finding clear alterations in myosin II (Sqh) localization in both *Rho1* (*Drosophila* RhoA) and *Rok* (*Drosophila* ROCK) mutants (Fig. 4, E–G‴). We reasoned that a phosphomimetic form of the myosin II (*Sqh^E20E21*, hereafter *Sqh^EE*; Winter et al., 2001) that bypasses Eph/Rok-dependent phosphorylation would be correctly located in *Eph* mutants. However, strong defects in myosin II Sqh^EE localization were still observed on an *Eph* mutant background, the same phenotype found when *Ephrin* was specifically down-regulated in the optic lobe NE (Fig. 4, H–J‴). Thus, Rok is not sufficient to activate myosin II in the absence of Eph.

Eph controls mitotic spindle orientation through aPKC activity–dependent myosin II regulation

In addition to Eph/Rho kinase–dependent phosphorylation, aPKC activity is essential to make myosin fully functional in some contexts (Wang and Riechmann, 2007; Kishikawa et al., 2008). Thus, we analyzed the distribution of active myosin II (Sqh^EE) on an *aPKC^CAAXDN* (kinase dead) mutant background, again finding clear alterations in its distribution (Fig. 5, B–C‴). This result suggested that Eph signaling in the optic lobe NE might act through aPKC, which in turn impinges on myosin functionality (Fig. 5 A). To test this possibility, we expressed a constitutively activated form of aPKC (aPKC^ΔN) in *Eph* mutant neuroepithelia, rescuing the apical distribution of active myosin II (Sqh^EE; Fig. 5, D–E‴). Moreover, the defects in the subapical region observed in *Eph* mutants at early stages (Fig. 2, C–D″) were also rescued by aPKC^ΔN on this active myosin II (Sqh^EE) genetic background (Fig. S3). Thus, Eph is required for aPKC

activation in the optic lobe NE, an activity that is essential for myosin II (Sqh) full functionality. We next checked whether the inactivation of aPKC in *Eph* mutants, and the consequent impairment of myosin II functionality, was responsible for the failures in mitotic spindle orientation observed in *Eph* mutants. The expression of the kinase-dead form of aPKC (*aPKC^CAAXDN*) in neuroepithelial cells provoked mitotic spindle alterations similar to those found in *Eph* and myosin II (*Sqh^AA*) mutants (Fig. 5 F). In addition, *aPKC^CAAXDN* mutants also showed defects in the INM process (Fig. 5 G). Moreover, both the mitotic spindle misorientation and the INM phenotypes of *Eph* mutants were rescued by aPKC^ΔN (Fig. 5, H and I). Hence, Eph controls mitotic spindle orientation and INM through aPKC activity–mediated myosin II regulation.

Core components of the mitotic spindle orientation machinery mislocalize in dividing *Eph* neuroepithelial cells

The activity of aPKC was impaired in *Eph* mutants, in turn affecting the distribution of myosin II (Sqh). Given that aPKC is involved in linking cortical polarity with the machinery required for mitotic spindle orientation in some epithelia (Hao et al., 2010; Durgan et al., 2011; Guilgur et al., 2012), we wondered whether the localization of these spindle regulators would be affected at mitosis in *Eph* mutants. We first examined Dlg1, which is required for spindle orientation in different cell types (Bellaïche et al., 2001; Johnston et al., 2009; Bergstralh et al., 2013b) and whose distribution was drastically altered in the neuroepithelial cells of the *Eph^x652* optic lobes at late L3 (Fig. 1, C–D′). While Dlg1 always presented a basolateral distribution at metaphase in control mitotic cells (*n* = 11) at early L3, in *Eph^x652* mitotic mutant cells Dlg1 was expanded apically in six of nine metaphases analyzed (Fig. 6, A–B′). Moreover, Dlg1 distribution was similarly affected in the neuroepithelial cells of myosin II (*Sqh^AA*) mitotic mutants (five cells with defects of eight metaphases analyzed; Fig. 6, C and C′). In addition, constitutively active aPKC (aPKC^ΔN) on an active myosin (Sqh^EE) and *Eph* mutant background rescued to a great extent the normal Dlg1 distribution. Neither aPKC^ΔN nor Sqh^EE alone rescued the Dlg1 phenotype in *Eph* mutants, further supporting the relevance of both aPKC and Rok downstream of Eph to fully activate myosin II (Sqh; Fig. S4). To directly test the role of Dlg1 in the orientation of the mitotic spindle in the optic lobe NE, we analyzed *dlg1^18* homozygotes, detecting significant spindle orientation defects at early L3 (Fig. 6 D).

We also wanted to analyze the localization of Mud/NuMA in *Eph* mutants, one of the most conserved spindle orientation regulators in different contexts and species (di Pietro et al., 2016). In control neuroepithelial cells, Mud was located at lateral membranes at pro-metaphase, and it was strongly enriched at centrosomes (Fig. 6, E–E‴). No apparent differences in this Mud enrichment at centrosomes were observed in *Eph^x652* or myosin II (*Sqh^AA*) mutant mitotic neuroepithelial cells at this stage, although there was a significant loss of Mud at the membrane. Indeed, in contrast to control cells (*n* = 7), Mud became mostly cytoplasmic on these mutant backgrounds in all pro-metaphase cells analyzed (*n* = 4 and *n* = 11, respectively; Fig. 6, F–G‴). We reasoned that the mislocalization of Mud could
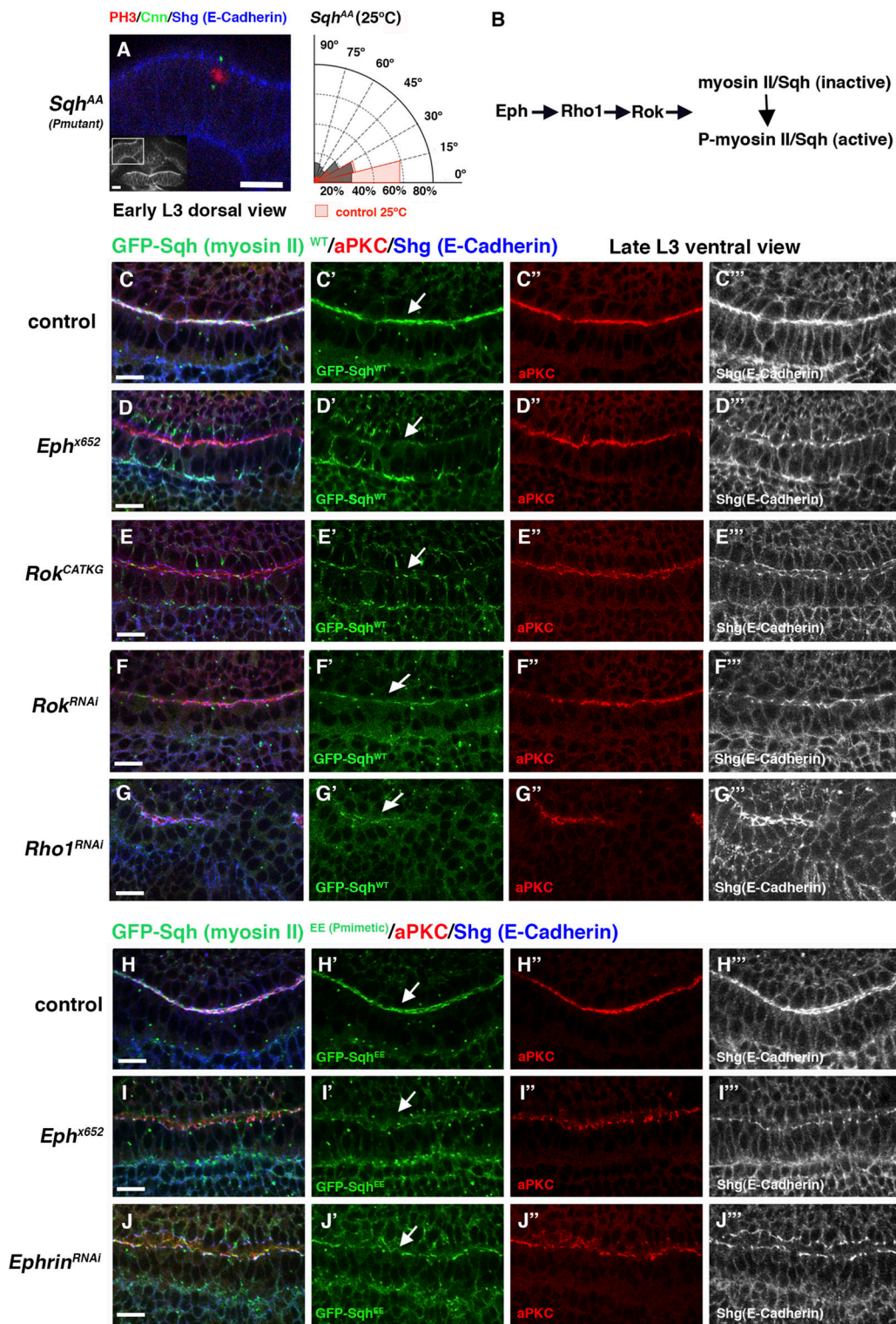
Figure 4. **Eph controls spindle orientation by regulating myosin II. (A)** A phosphomutant form of myosin II (Sqh^{AA}) shows defects in mitotic spindle orientation in neuroepithelial cells. In the diagram, the mutant phenotype is shown in gray and the control (25°C) in red. A χ^2 test was used to compare the control ($n = 72$ mitotic cells) and mutant myosin II (Sqh^{AA}; $n = 54$) populations; $P < 0.001$. **(B)** Eph can act through Rho signaling to phosphorylate and activate myosin II (Sqh). **(C–G''')** The localization of myosin II (Sqh^{WT}) is disrupted in Eph^{x652}, Rok, and Rho1 mutant neuroepithelia compared with control neuroepithelia (arrows). The panels show late L3 stage. **(H–J''')** A phosphomimetic form of myosin II (Sqh^{EE}) still shows localization defects in Eph^{x652} and in $Ephrin^{RNAi}$ mutant neuroepithelia (arrows). The NE-specific Gal4 line c855 was used as a driver to express all the UAS transgenes (i.e., Rok^{CAT-KG}, Rok^{RNAi}, $Rho1^{RNAi}$, and $Ephrin^{RNAi}$). Scale bars, 10 μm.
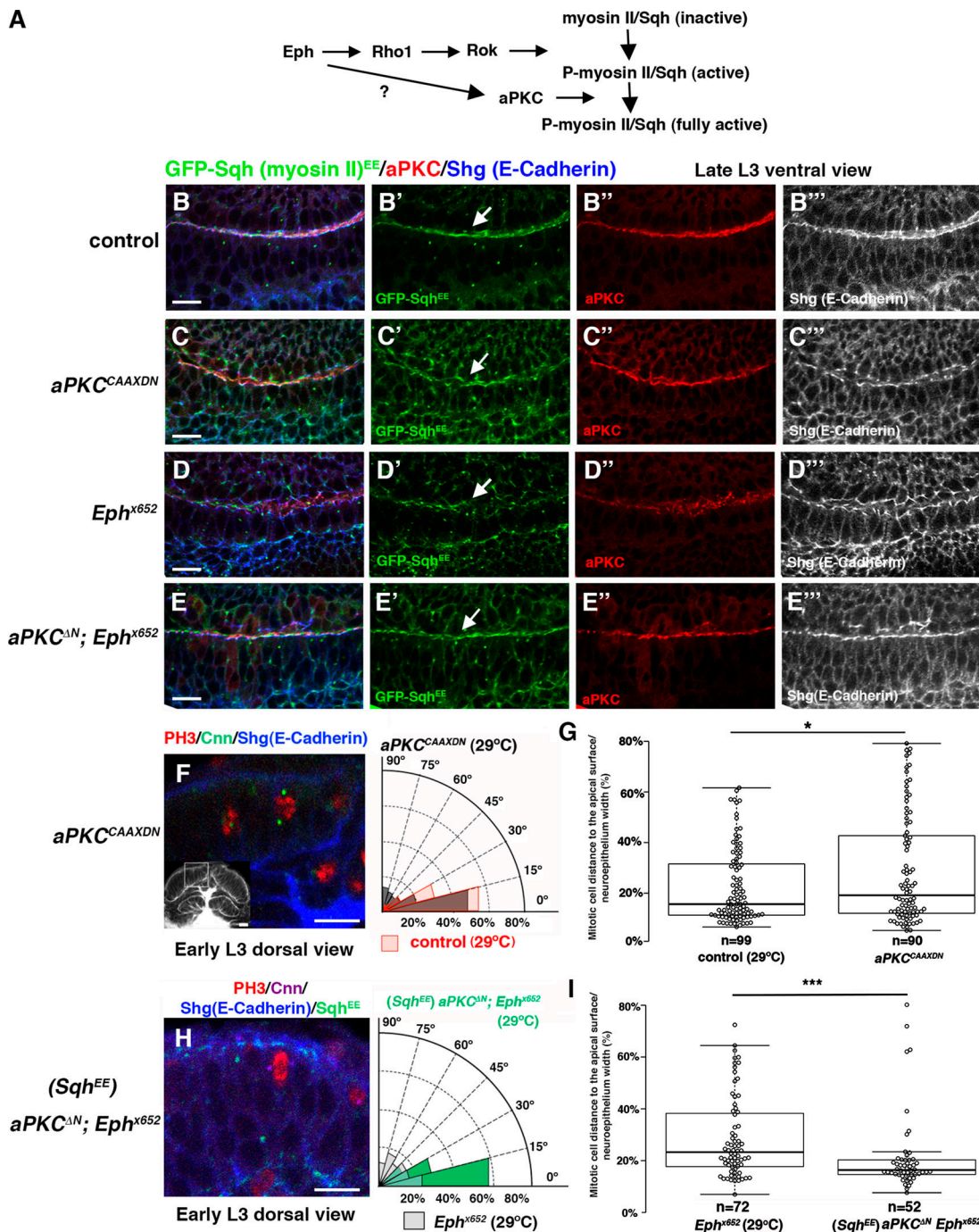
Figure 5. **Eph controls mitotic spindle orientation through aPKC activity–dependent myosin II regulation. (A–E''')** Eph could act through aPKC to fully activate myosin II (Sqh; A). The localization of phosphomimetic myosin II (Sqh^{EE}) is disrupted on an aPKC^{CAAXDN} (kinase dead) mutant background (B–C'''), and a constitutively activated form of aPKC (aPKC$^{\Delta N}$) rescues the defective apical localization of Sqh^{EE} found in Eph^{x652} mutant neuroepithelia (D–E'''). **(F and G)** The expression of a kinase-dead form of aPKC (aPKC^{CAAXDN}) in neuroepithelial cells shows mitotic spindle alterations (F, $n = 73$, $P < 0.01$; $n = 75$ control mitotic cells) and INM defects (G, $n = 90$, *, $P < 0.05$; $n = 99$ control cells). The Gal4 line c855 was used as a driver. In F, the mutant phenotype is shown in gray and the control (29°C) in red. **(H and I)** A constitutively activated form of aPKC (aPKC$^{\Delta N}$) rescues the mitotic spindle orientation defects ($n = 56$ mitotic cells; $P < 0.0001$ in H) and INM failures ($n = 52$ mitotic cells; ***, $P < 0.001$ in I) found in Eph^{x652} mutant neuroepithelia ($n = 80$ and $n = 72$ cells, respectively). Quantification of the Eph defects in H are shown in gray and the rescue in green in the diagram. A χ^2 test was used to analyze the data in F and H. The data in G and I were analyzed with a Mann–Whitney U test; the central lines show the medians, and the box limits indicate the lower and upper quartiles as determined with R software. Scale bars, 10 µm.

contribute to the spindle phenotype observed in Eph^{x652} and myosin II mutants (Sqh^{AA}). In fact, mud down-regulation in neuroepithelial cells produced significant defects in spindle orientation compared with control cells (Fig. 6 H). Hence, both Dlg1 and Mud mislocalization in Eph mutants could account for the spindle phenotype observed in these mutants.
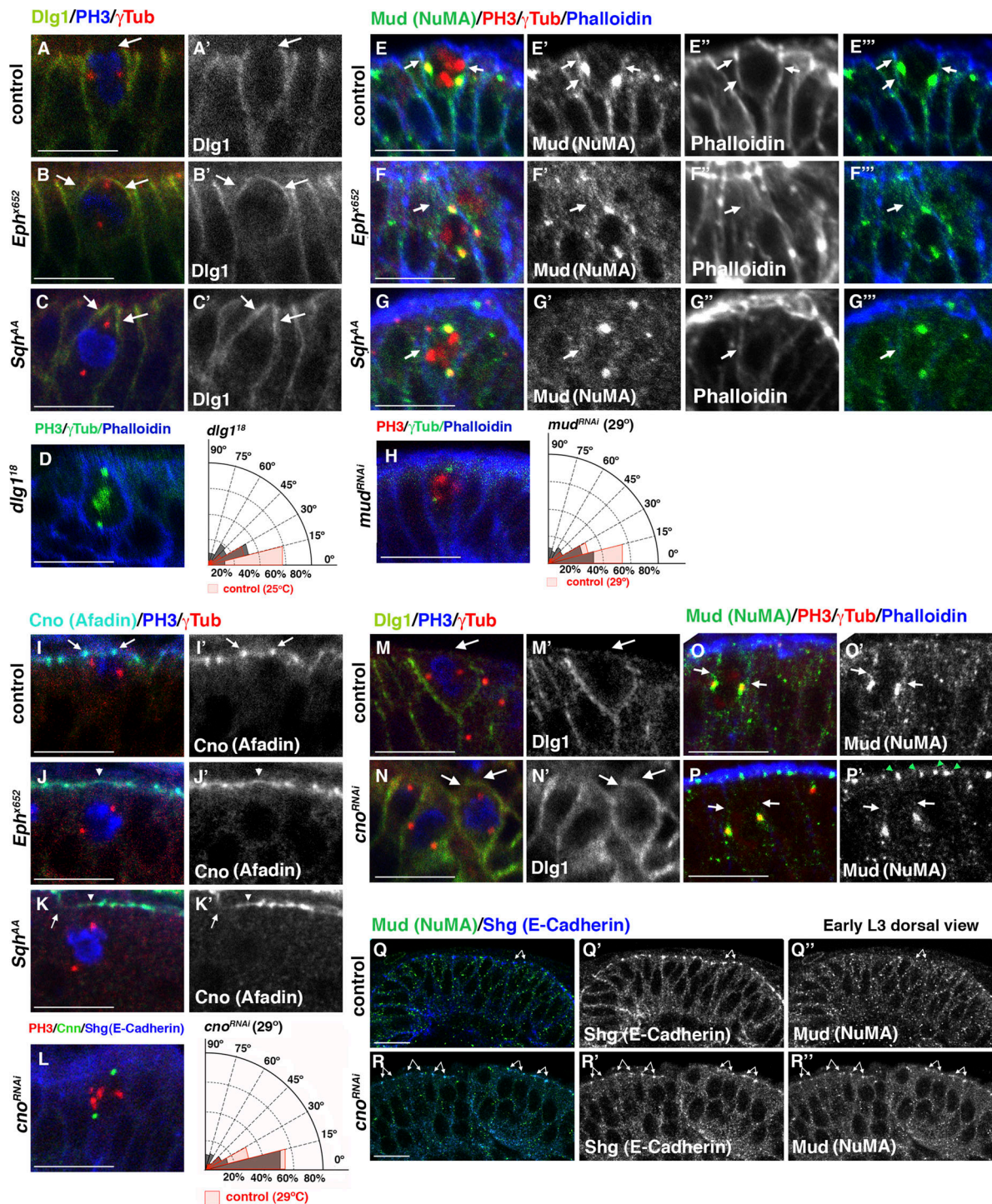
Figure 6. Core components of the mitotic spindle orientation machinery mislocalize in dividing *Eph* neuroepithelial cells. (A–C′) Dlg1 is redistributed cortically in *Eph^x652* and *Sqh^AA* mitotic mutant cells at the early L3 stage. White arrows point to an anomalous apical localization of Dlg1 in B–C′, compared with the lack of apical Dlg1 in control cells (A and A′). **(D)** *dlg1^18* early L3 mutant homozygotes show a significant number of perpendicular or oblique divisions (>30°; *n* = 44, P < 0.0001), relative to the control mitotic cells (*n* = 72). **(E–G′″)** Mud is present in the lateral membranes (arrows) of control mitotic neuroepithelial cells (E–E′″) and is highly enriched at centrosomes (labeled with γ-Tub) at pro-metaphase (yellow dots). Mud is mostly cytoplasmic in *Eph^x652* (F–F′″) and *myosin II* (*Sqh^AA*; G–G′″) mitotic mutant cells at this stage, while its accumulation at centrosomes is not affected. **(H)** Down-regulation of *mud* in optic lobe neuroepithelia shows a significant number of perpendicular or oblique divisions (>30°; *n* = 41, P < 0.01), compared with control mitotic cells (*n* = 75) at early L3. **(I–K′)** Cno is enriched at AJs in control mitotic neuroepithelial cells (arrows in I and I′), and it is cortically redistributed (arrowheads in J–K′) or shows cortical gaps (arrows in K and K′) in *Eph^x652* and *myosin II* (*Sqh^AA*) mitotic mutant cells at early L3. **(L)** The down-regulation of *cno* in optic lobe neuroepithelia causes a significant number of vertical divisions (>30°; *n* = 76, P < 0.05), compared with the control mitotic cells (*n* = 75). **(M–P′)** The lateral localization of both Dlg1 (M–N′) and Mud (O–P′) was diminished in mitotic neuroepithelial cells in which *cno* was down-regulated relative to control cells (arrows), and Mud is enriched at what seem to be the AJs (green arrowheads in P′). Mud enrichment at centrosomes is not apparently affected at this stage. **(Q–R′)** Mud is enriched at AJs along with Shg

(E-cadherin) in *cno* mutant neuroepithelia (arrows in R–R″) compared with the occasional presence of Mud at AJs in control neuroepithelia (arrows in Q–Q″). In all quantifications, the spindle mutant phenotype is shown in gray and the control in red, and a χ^2 test was used to compare population values. The NE-specific Gal4 line c855 was used to drive the expression of both *mud^{RNAi}* and *cno^{RNAi}*. Scale bars, 10 µm.

Cno and its vertebrate homologue Afadin regulate mitotic spindle orientation in different cell types both in vivo (Speicher et al., 2008; Rakotomamonjy et al., 2017) and in cell culture (Johnston et al., 2013; Carminati et al., 2016). In addition, Cno is required for the cortical recruitment of Mud/NuMA and Dlg1 in mitotic NBs (Speicher et al., 2008; Keder et al., 2015). Thus, we wondered whether Cno localization would also be affected in mitotic *Eph^{x652}* optic lobe neuroepithelial cells. While in control neuroepithelia Cno is always enriched at AJs (n = 6 mitotic cells; Fig. 6, I and I′), in *Eph^{x652}* mutants the cortical distribution of Cno was altered (i.e., it was either apically expanded or showed cortical gaps) in 7 of 10 mitotic cells analyzed (Fig. 6, J and J′). A similar phenotype was observed in 8 of 10 myosin II mutant (*Sqh^{AA}*) mitotic cells (Fig. 6, K and K′). In addition, we found that the down-regulation of *cno* in optic lobe neuroepithelial cells caused a misorientation of mitotic spindles (Fig. 6 L). Finally, we assessed the localization of both Dlg1 and Mud in mitotic neuroepithelial cells in which Cno was down-regulated. Dlg1 was apically expanded in 10 of 16 *cno* mitotic mutant cells (Fig. 6, M–N′), while the localization of Mud to lateral membranes was strongly diminished at all pro-metaphases analyzed (n = 6) relative to control cells (n = 7; Fig. 6, O–P′). We also observed an enrichment of Mud at what seemed to be the AJs in some *cno* mutant neuroepithelia (Fig. 6, P and P′). To confirm this, we used Shg (E-cadherin) as a marker of the AJs, and in two of eight *cno* mutant neuroepithelia (from eight different brains), Mud was clearly enriched at AJs (Fig. 6, Q–R″). In control neuroepithelia, Mud was occasionally observed at AJs along with Shg (E-cadherin), yet it was never clearly enriched in them (n = 6 brains; Fig. 6, Q–R″). Hence, we conclude that the restriction of Cno to the AJs of neuroepithelial cells in normal conditions might contribute to confine Dlg1 and Mud to lateral membranes.

Eph signaling regulates cell proliferation, inhibiting the PI3K–Akt1 pathway through Rok in the optic lobe NE

The optic lobes in *Eph^{x652}* brains were consistently larger than in WT brains (Fig. 7, A–C). In fact, compared with control brains, *Eph^{x652}* optic lobe neuroepithelia displayed overgrowth at the mid-late L3 stage (Fig. 7, D–F), which was accompanied by an increase in the rate of neuroepithelial cell proliferation in *Eph^{x652}* mutants (Fig. 7, G–I) along with a decrease in apoptosis at early L3 (Fig. 7, J, M, and P). At mid-late L3 stage, the levels of apoptosis were similar to those in control neuroepithelia (Fig. 7, K, N, and L–P), although the rate of cell proliferation was still higher in *Eph^{x652}* mutants (Fig. 7, Q–T). Eph receptors are functionally linked to Rho small GTPases (Wahl et al., 2000; Noren and Pasquale, 2004; Lisabeth et al., 2013) and impaired Rho signaling has in turn been associated with an activation of the PI3K–Akt signaling pathway, a major regulator of cell proliferation (Lawlor and Alessi, 2001; Scheid and Woodgett, 2001; Luo et al., 2003; Li et al., 2005; Hopkins et al., 2014; Chang et al., 2016). We found that the expression of PI3K in the optic lobe NE

was associated with an overproliferation phenotype similar to that of *Eph^{x652}* mutants (Fig. 8 A). Hence, we tested the levels of Akt activation in *Eph^{x652}* mutant brains. Compared with control brains, *Eph^{x652}* mutant brain extracts revealed higher levels of phospho-Akt1 (pAkt1) in Western blots (WBs), as also seen in *Eph^{KD}* (kinase dead) mutant extracts (Fig. 8 B). Moreover, the overgrowth phenotype in *Eph^{x652}* neuroepithelia was rescued by specifically expressing *Akt1^{RNAi}* or *PI3K^{RNAi}* in this tissue (Fig. 8, C and D). The spindle phenotype in *Eph^{x652}* neuroepithelial cells was also partially rescued by down-regulating Akt1 signaling, although many vertical divisions (>30°) still persisted (i.e., 43.5% of the total divisions, n = 92, compared with 61.2% in *Eph^{x652}* mutants, n = 80, and 17.3% in control divisions, n = 75; Fig. 8 E; see also Discussion). Finally, to determine whether Rho signaling was involved in this Akt1 regulation, we analyzed both neuroepithelial cell proliferation as well as the levels of pAKT1 in *Rok^{CATKG}* kinase dead and *Rok^{RNAi}* mutants, which displayed similar phenotypes to those shown by *Eph* mutants (Fig. 8, F and G). Moreover, a constitutively activated form of Rok (Rok^{CAT}) suppressed the overgrowth phenotype showed by *Eph^{x652}* mutants (Fig. 8 H). We conclude that Eph signaling regulates cell proliferation in the optic lobe NE through activation of Rok, which in turn inhibits PI3K–Akt1 signaling pathway (see also below).

Discussion

Different intrinsic and, to an apparently much lesser extent, extrinsic mechanisms tightly coordinate the correct orientation of the spindle during epithelial cell division (Morin and Bellaïche, 2011; Werts and Goldstein, 2011; Lu and Johnston, 2013; Williams and Fuchs, 2013). This process is essential to maintain epithelial morphology and to prevent hyperplasia (McCaffrey and Macara, 2011; Pease and Tirnauer, 2011). In fact, robust mechanisms have evolved to avert the consequences that a failure to correctly align the spindle would cause (Guilgur et al., 2012; Nakajima et al., 2013; Bergstralh et al., 2015).

Here we reveal Ephrin–Eph signaling to be a novel extrinsic mechanism that controls spindle orientation, influencing the regulation of intrinsic cues in the *Drosophila* optic lobe NE. Moreover, the loss of Eph signaling entails an up-regulation of the PI3K–Akt1 pathway and an ensuing increase in cell proliferation in this tissue. Both events seem to be independently regulated by Eph signaling, although both processes depend on Rok activation by Eph. From this point onwards, spindle orientation relies on Eph signaling–dependent aPKC activity, whereas cell proliferation is controlled by Eph/Rok-dependent inhibition of PI3K–Akt1 signaling pathway.

As a result of the data obtained, we propose a working model in which both reverse and forward Eph signaling would operate between optic lobe neuroepithelial cells (Fig. 9). On one hand, reverse Eph-ephrin signaling at the level of the subapical region would activate aPKC. Indeed, the existence of such signaling was
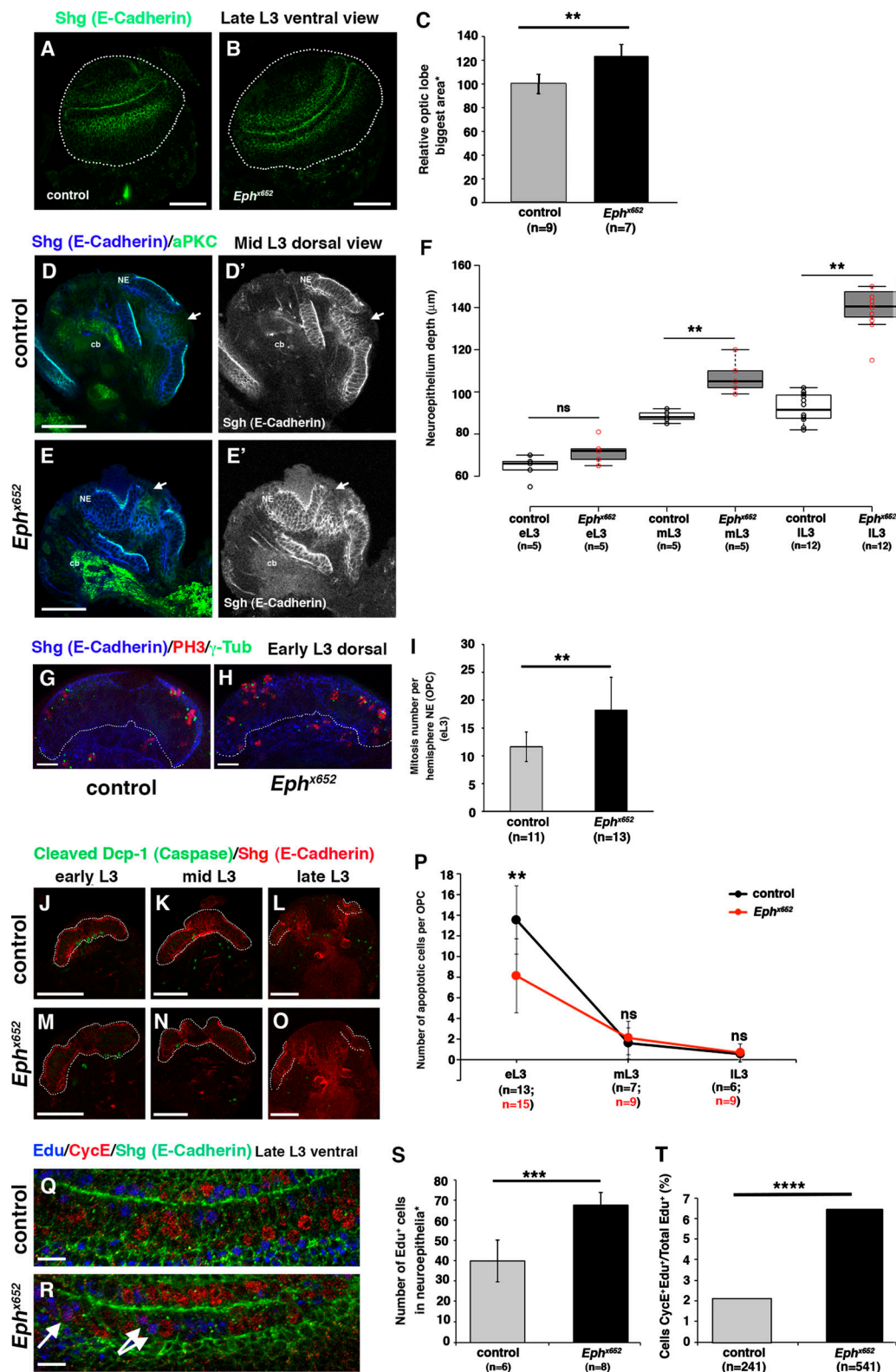
Figure 7. **Eph signaling regulates cell proliferation in the optic lobe NE. (A–C)** Eph^{x652} mutant optic lobes (B) are bigger than control lobes (A). **(C)** In both control (n = 9) and Eph^{x652} mutant (n = 7) hemispheres, the plane of focus showing the largest area was chosen to calculate the relative increase (%) in Eph^{x652} mutants. The data were analyzed with an unpaired two-tailed Student's t test (**, P < 0.01); error bars show the SD. **(D–E')** Eph^{x652} mutant optic lobe neuroepithelia (stained with Shg/E-cadherin) already display overgrowth at the mid L3 stage (E and E') compared with control neuroepithelia (D and D'). As a reference, the white arrow indicates the lamina side of the optic lobe NE; cb, central brain. **(F)** Quantification of the NE depth from early to late L3 in Eph^{x652} mutant and control brains. Significant overgrowth is evident in Eph^{x562} mutants from mid L3 stage (**, P < 0.01; ns, not significant). The data were analyzed with an ANOVA test, and the central lines represent the median, error bars indicate the SEM, and box limits indicate the lower and upper quartiles, as

determined by R software. **(G–I)** Z-projections of 10-slice confocal stacks of the indicated genotypes are shown (G and H). *Eph*^x652 mutants show a significant increase in the number of neuroepithelial cell mitosis at early L3 compared with the control (I; **, P < 0.01). Mitoses were quantified in the OPC of each brain hemisphere, and the data were analyzed by an unpaired two-tailed Student's *t* test, with the error bars indicating the sd. **(J–P)** In *Eph*^x652 mutants, there is a decrease in apoptosis in the NE at the early L3 stage relative to the control (**, P < 0.01; J, M, and P). The levels of apoptosis are similar in the mutant and the control at mid-late L3 stage (K, L, and N–P). Statistical significance was assessed by an ANOVA test, and error bars indicate SD. **(Q–T)** The rate of cell proliferation is significantly higher in *Eph*^x652 mutant neuroepithelia at late L3 than in control neuroepithelia (Q–S; ***, P < 0.001). The data were analyzed by an unpaired two-tailed Student's *t* test, and the error bars indicate the SD. The percentage of Edu⁺ cells that are entering the cycle (CycE⁺) is significantly higher in *Eph*^x652 neuroepithelia than in controls (Q, R, and T; ****, P < 0.0001). The data were analyzed with a Z test to compare two proportions. Scale bars, 10 µm in G, H, Q, and R, and 50 µm in the rest of the panels.

previously shown to regulate tight junctions in *Xenopus* embryos through Par-6, which as part of the Par complex (Par-6/aPKC/Cdc42) ultimately leads to aPKC activation (Lee et al., 2008). Intriguingly, we observed a collapse of the subapical region (the equivalent in *Drosophila* of vertebrate tight junctions) in the *Eph* mutant optic lobe neuroepithelial cells. Moreover, a constitutively activated form of aPKC on an *Eph* mutant background rescued this collapse in the subapical region. In addition, constitutively active aPKC rescued the distribution of phosphomimetic myosin II (Sqh^EE), as well as the spindle orientation and deficient INM found in *Eph* mutant neuroepithelia. It is worth noting that constitutively active aPKC rescued the localization defects of Dlg1 in dividing Eph mutant cells in combination with active myosin II (Sqh^EE), but not in the presence of inactive myosin II (Sqh^WT; Fig. S4). This result strongly supports the requirement of both aPKC and Rok to make myosin II fully functional. *myosin II* mutants (*Sqh*^AA) had defects in the subapical region and in the spindle orientation similar to those found in *Eph* mutants, and failures in INM have previously been described when the apico-basal distribution of myosin II is altered (Rujano et al., 2013). Hence, myosin II seems to lie at the central regulatory node of all these processes. Interestingly, Ephrin B1 reverse signaling regulates apical adhesion of neural progenitors at the ventricular zone of the mouse developing cortex. In this context, Ephrin B1 induces adhesion of apical progenitors to the extracellular matrix by promoting the apical localization of integrin β1 (Arvanitis et al., 2013). Given that β integrin/Mys localizes basally in the *Drosophila* optic lobe NE, Ephrin reverse signaling would act, in principle, through aPKC activation to organize the apical/subapical region in this NE. Nevertheless, the decreased levels of β integrin/Mys we detected in *Eph* mutant neuroepithelial cells might also lead to defective adhesion to the extracellular matrix in this system.

On the other hand, PI3K–Akt1 signaling would be inhibited by forward Ephrin–Eph signaling through Rho1/Rok activation. Indeed, there was an increase in pAkt1 in *Rok* mutant brain extracts, as well as in cell proliferation in *Rok* mutant optic lobe neuroepithelia. Moreover, a constitutively activated form of Rok suppressed the *Eph* mutant overproliferation phenotype. Activation of Rho GTPases and the ensuing activation of Rho kinases downstream of Eph receptors has been well documented, especially in neuronal growth cones (Wahl et al., 2000; Shamah et al., 2001; Lisabeth et al., 2013). Our results, along with previously published data, suggest that Rok acts upstream of PI3K–Akt1 (Sordella et al., 2003; Furukawa et al., 2005; Chang et al., 2016). In fact, ROCK phosphorylates and activates the Phosphatase and tensin homologue PTEN, an inhibitor of PI3K–Akt signaling pathway, in mammalian cells. Phosphorylated PTEN inhibits the recruitment of Akt by PI3K and thus represses proliferation (Li et al., 2005; Hopkins et al., 2014). The down-regulation of Akt1 on an *Eph* mutant background rescued the *Eph* overproliferation phenotype, and intriguingly, it also partially rescued the *Eph* spindle phenotype. Akt is involved in microtubule interactions and spindle orientation in some contexts (Buttrick et al., 2008; Buttrick and Wakefield, 2008). Based on our results, Eph would inhibit Akt signaling in normal circumstances, and hence, in principle Akt would not be required for spindle alignment in optic lobe neuroepithelial cells. As Akt was overactivated in *Eph* mutants, this could interfere with spindle microtubules and contribute to the defects in spindle orientation. In such a scenario, Akt down-regulation could partially rescue the spindle alignment defects, as observed. However, in this situation many more vertical divisions were still detected, while the rescue of the spindle phenotype of *Eph* mutants by aPKC activation was much more robust (see Results). Along with the inhibition of Akt by Eph detected in WT neuroepithelial cells, these observations strongly suggest that Eph regulating myosin II through aPKC activation is the main driver orienting the spindle in this context.

Finally, the loss of Eph signaling in the optic lobe NE altered the localization of known intrinsic mitotic spindle regulators in other cell types, including Dlg1, Mud/NuMA, and Cno/Afadin, the loss of which also led to spindle orientation defects in this NE. aPKC activity, which was disrupted in *Eph* mutants, is required for the correct orientation of the spindle in some epithelia. For example, aPKC phosphorylates Pins, excluding it to the apical membrane and favoring its lateral localization in *Drosophila* imaginal disc epithelia (Guilgur et al., 2012). In NBs and S2 cells, Pins binds to Cno, Mud, and Dlg1 for orchestrating the correct alignment of the spindle (Bowman et al., 2006; Izumi et al., 2006; Siller et al., 2006; Speicher et al., 2008; Johnston et al., 2009; Wee et al., 2011). Hence, it is possible that aPKC may not phosphorylate and exclude Pins from the apical membrane in *Eph* mutant neuroepithelial cells. This might explain, at least in part, the apically expanded domains of Dlg1 and Cno in *Eph* mutants. However, alterations to the actomyosin cortex, which is compromised in *Eph* mutants, must also be directly responsible for the mislocalization of these spindle regulators, particularly as myosin II (*Sqh*^AA) mutants showed similar phenotypes to *Eph* mutants. In addition, Mud was not detected apically in *Eph* mutants. In fact, Mud was enriched in the cytoplasm, in detriment to its lateral distribution at pro-metaphase, in both *Eph* and myosin II (*Sqh*^AA) mutants. This lateral distribution of Mud was also compromised by down-regulating *cno* in the NE.
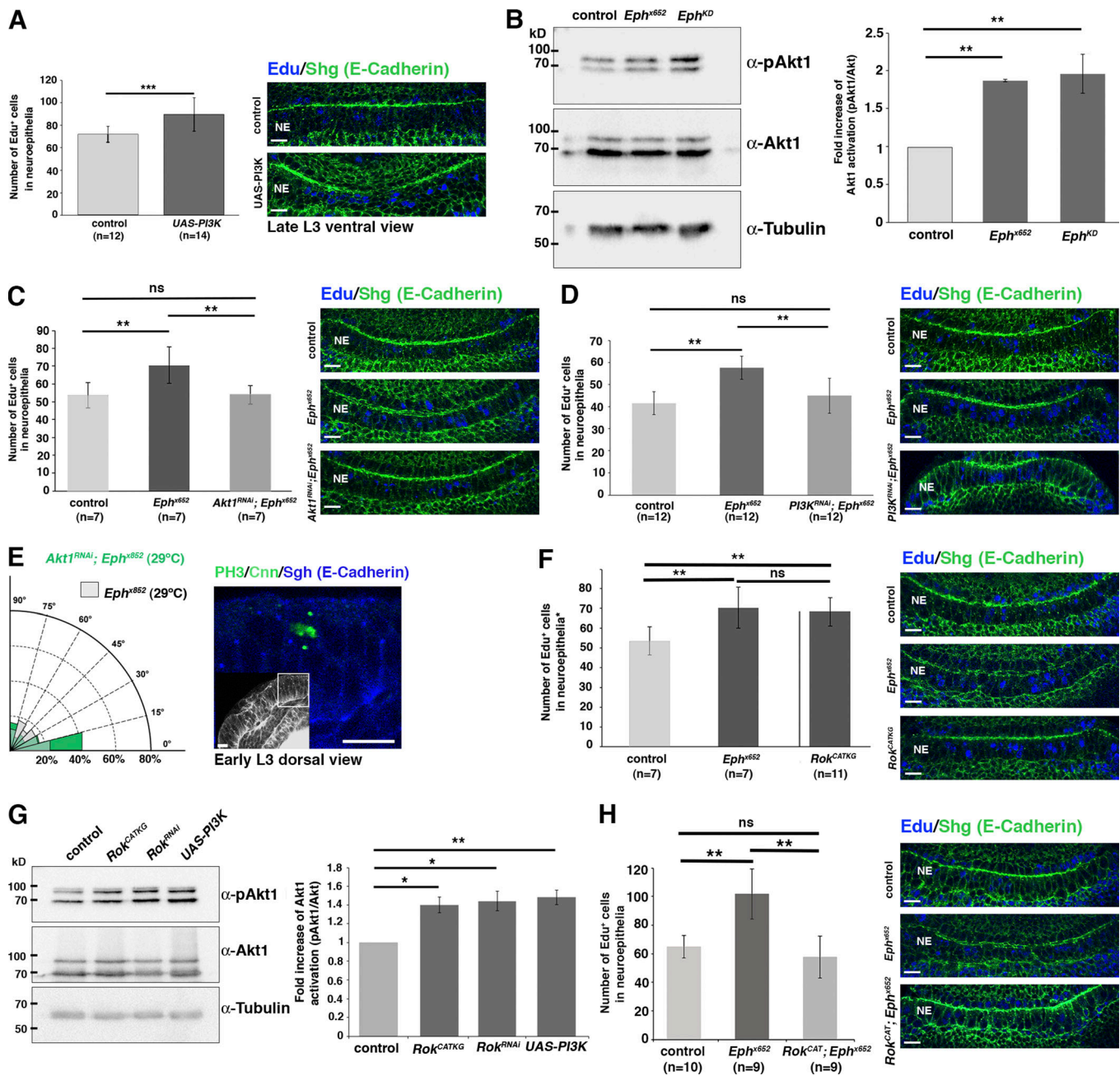
Figure 8. **Eph signaling regulates cell proliferation inhibiting the PI3K–Akt1 pathway through Rok in the optic lobe NE. (A)** Overexpressing PI3K under the NE Gal4 driver c855 produces a significant increase in cell proliferation (*n* = 14 hemisphere OPCs from 11 different brains; ***, P < 0.001) relative to control neuroepithelia (*n* = 12 hemisphere OPCs from eight different brains). An unpaired two-tailed Student´s *t* test was used to analyze data, and the error bars indicate SD. **(B)** WB of larval brain lysates from the indicated genotypes probed for pAkt1, the antibody detecting two Akt1 isoforms (66 and 85 kD). A significant increase in pAkt1 levels is found in both *Eph^x652* (**, P < 0.01) and in *Eph^KD* (**, P < 0.01) mutants. Data from three independent experiments were analyzed by ANOVA, and the error bars indicate the SEM. **(C)** The overgrowth phenotype in *Eph^x652* neuroepithelia (*n* = 7 hemisphere OPCs from five different brains) relative to the controls (*n* = 7 from four brains) is rescued by specifically expressing *Akt1^RNAi* in the NE (*n* = 7 from four brains; **, P < 0.01). The Gal4 line c855 was used as a driver, and the data were analyzed by ANOVA with the error bars indicating the SD. **(D)** The overgrowth phenotype of *Eph^x652* neuro-epithelia (*n* = 12 hemisphere OPCs from nine different brains) compared with the control (*n* = 12 from nine brains) is rescued by specifically expressing *PI3K^RNAi* in the NE (*n* = 12 from seven brains; **, P < 0.01). The Gal4 line c855 was used as a driver, and the data were analyzed by ANOVA with error bars indicating the SD. **(E)** The spindle phenotype of *Eph^x652* mitotic neuroepithelial cells (*n* = 80) was partially rescued by down-regulating Akt1 signaling in the NE (*n* = 92; *, P < 0.05), with a high percentage of vertical divisions (>30°) still present (see also the main text); a χ² test was used to compare populations, and the Gal4 line c855 was used as a driver. **(F)** *Rok^CATKG* kinase dead mutants (*n* = 11 hemisphere OPCs from seven different brains) phenocopy the overgrowth phenotype of *Eph^x652* mutant neuroepithelia (*n* = 7 from five brains). The control and *Eph^x652* data are the same as in C, as they form part of the same experiment (i.e., control, *Eph^x652*, *Akt1^RNAi Eph^x652*, and *Rok^CATKG*). As in C, the data were analyzed by ANOVA, and the error bars indicate the SD. **(G)** WB of larval brain lysates of the indicated genotype showing pAkt1 levels. Two isoforms of Akt1 are detected by the antibody (66 and 85 kD). A significant increase in pAkt1 levels is found in both the *Rok^CATKG* (*, P < 0.05) and *Rok^RNAi* (*, P < 0.05) mutants. The data from three different experiments were analyzed by ANOVA, and the error bars indicate the

SEM. **(H)** The overgrowth phenotype of Eph^{x652} neuroepithelia ($n = 9$) compared with control neuroepithelia ($n = 10$) is suppressed by a constitutively activated form of Rok (Rok^{CAT}; $n = 9$; **, $P < 0.01$). The Gal4 line c855 was used as a driver, and the data were analyzed by ANOVA with the error bars indicating the SD. Scale bars, 10 µm.

Intriguingly, in these circumstances Mud was enriched at AJs in some of the larval brain neuroepithelia analyzed. Dlg1 was apically expanded in most dividing *cno* mutant cells. Thus, this *cno* mutant phenotype would suggest that Cno restriction to AJs might help confine Mud and Dlg to the lateral cortex in normal neuroepithelia. However, further work will be necessary to clarify this issue. Moreover, given the general conservation of spindle regulators in different cell types and organisms, it will be interesting to determine whether Eph signaling performs a similar function in other epithelia, both in *Drosophila* and in vertebrates, to modulate mitotic spindle alignment.

Materials and methods

Drosophila strains and genetics
All the fly stocks used were from the Bloomington *Drosophila* Stock Center (BDSC) and the Vienna *Drosophila* Resource Center (VDRC), unless otherwise stated: *yw* (Speicher et al., 2008); Eph^{x652} (Boyle et al., 2006); Eph^{KD} (Dr. Richard E. Dearborn, Albany College of Pharmacy and Health Sciences, Albany, NY); $dlg1^{18}$ (BDSC: 36279); *UAS-Eph-Myc* (Scully et al., 1999); *UAS-Eph^{RNAi}* (VDRC: KK105139); *C855a-Gal4* (BDSC: 6990); *GFP-Sqh^{WT}, GFP-Sqh^{EE},* and *GFP-Sqh^{AA}* (Dr. Renata Basto, Institute Curie, PSL Research University, CNRS, Paris, France); *UAS-Rho1^{RNAi}* (BDSC: 9909); *UAS-Rok^{RNAi}* (BDSC: 28797); *UAS-Rok^{CAT-KG}* (BDSC: 6670); *UAS-Rok^{CAT}* (BDSC: 6668); *UAS-aPKC^{CAAXDN}* (Dr. Sol Sotillos, CABD, CSIC/JA/Universidad Pablo de Olavide, Seville, Spain); *UAS-aPKC^{ΔN}* (BDSC: 51673); *UAS-aPKC^{RNAi}* (VDRC: KK105624); *UAS-cno^{RNAi}* (VDRC: GD7769); *UAS-Akt1^{RNAi}* (VDRC: KK103703); *UAS-PI3K^{RNAi}* (VDRC: GD38985); *UAS-mud^{RNAi}* (BDSC: 38190); *UAS-Dp110^{CAAX}* (BDSC: 25908); and *Gal80^{ts}* (BDSC:

7108). The GAL4xUAS crosses were performed at 29°C except for the *Tub-GAl80^{ts}; C855a-Gal4; Eph^{x652} × GFP-Sqh^{EE} (or GFP-Sqh^{WT}) aPKC^{ΔN}; Eph^{x652}* cross, which was incubated for 3 d at 18°C and 1 d at 29°C (Fig. 5, H and I; and Figs. S3 and S4), and 2 d at 18°C followed by 3 d at 29°C (Fig. 5 E) before dissection. Similarly, the *Tub-GAl80^{ts}; C855a-Gal4 × UAS-PI3K^{CAAX}* (Fig. 8, A and G) and *Tub-GAl80^{ts}; C855a-Gal4; Eph^{x652} × UASPI3K^{RNAi}; Eph^{x652}* (Fig. 8 D) crosses were incubated for 2 d at 18°C and 3 d at 29°C before dissection.

Histology, immunofluorescence, and microscopy
Larval brains were dissected out in PBS and fixed with 4% PFA in PBT (PBS and Triton X-100 0.1%) for 20 min at room temperature with gentle rocking. For immunostaining with the rabbit anti-Cno antibody, the brains were fixed using the heat and methanol method (Miller et al., 1989) with small modifications. Briefly, dissected brains were incubated for 20 s at 80°C in buffer H (70 mM NaCl and 0.1% Triton X-100), followed by 5-min incubation on ice. The solution was then changed for PBT and incubated for another 5 min on ice. Embryos in Fig. S1 (D and E) were also fixed using the heat and methanol method; in this case, after the 5-min incubation on ice in buffer H, embryos were passed to heptane and treated with the same volume of methanol for devitelinization. From this point, both fixed brains and embryos were incubated in PBT for at least 30 min and then in PBT-BSA for 1 h before incubation with the corresponding primary antibody. For embryo staining with the anti-Eph antiserum (1:1,000; see below), a biotin anti-rabbit (Vector Laboratories) and the VectaStain Elite ABC HRP kit (Vector Laboratories) were used.

The primary antibodies used in this study were rabbit anti-Eph (1:500; see below), rat anti-DE-cadherin (1:100; Developmental
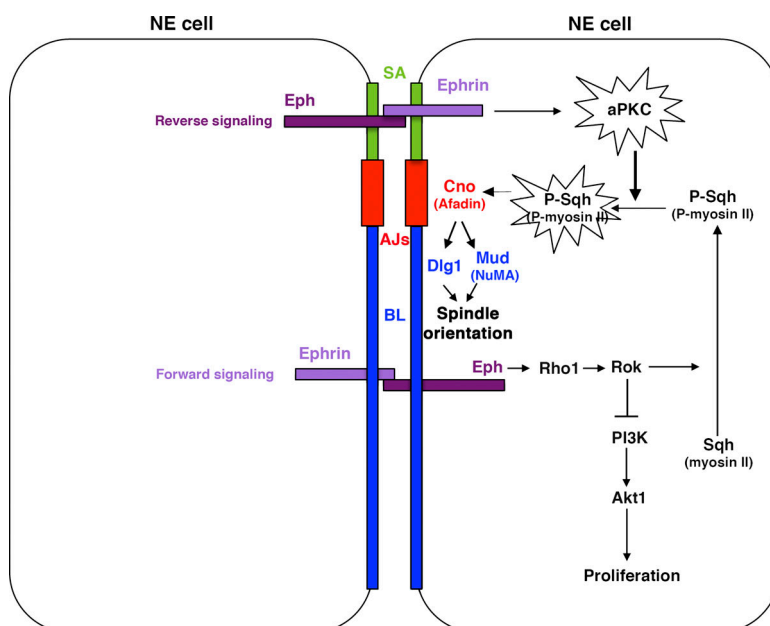

Figure 9. **Working model.** Two optic lobe neuroepithelial cells are represented in which the subapical region (SA) appears in green, the AJs in red, and the basolateral region (BL) in blue. Reverse Eph signaling at the level of the SA would be relevant for aPKC activation, and in turn, this would be key to fully activate P-myosin II (Sqh in *Drosophila*), which impinges on mitotic spindle orientation by contributing to the correct cortical localization of Cno, Dlg1, and Mud during mitosis. Forward Eph signaling would activate Rho-Rok signaling, which in turn would have two effects: (1) phosphorylate and activate myosin II (Sqh) and (2) keep the PI3K–Akt1 signaling pathway inhibited.

Studies Hybridoma Bank [DSHB]), rabbit anti-PatJ (1:2,000; Dr. Elisabeth Knust, Max-Planck Institute for Molecular Cell Biology and Genetics, Dresden, Germany), rabbit anti-PKCζ (1:100; Santa Cruz Biotechnology, sc-216), rabbit anti-Par6 (1:2,000; Dr. Juergen Knoblich, Institute of Molecular Biotechnology of the Austrian Academy of Sciences, Vienna, Austria), rabbit anti-Baz (1:1,000; Dr. Andreas Wodarz, Institute for Anatomy University of Cologne Medical School, Koln, Germany), rabbit anti-Cno (1:400; Speicher et al., 2008), mouse anti-Dlg1 (1:100; DSHB), rabbit anti-Mud (1:400; Dr. Fumio Matsuzaki, RIKEN Center for Developmental Biology, Chuo-ku, Kobe, Japan), mouse anti-Mys (1:100; DSHB), rabbit anti-Scrib (1:2,000; Dr. Chris Doe, Institute of Neuroscience, Howard Hughes Medical Institute, University of Oregon, Eugene, OR), guinea pig anti-Dpn (1:2,000; Rives-Quinto et al., 2017), rabbit anti-cleaved dDcp1 (1:100; Cell Signaling Technology, 9578), mouse anti-PH3 (1:2,000; Millipore, 05-806), rabbit anti-PH3 (1:1,000; Millipore, 06-570), rabbit anti-CycE (1:100; Santa Cruz Biotechnology, 33748), rabbit anti-Cnn (1:400; Dr. Thomas C. Kaufman, Indiana University, Bloomington, IN), and mouse anti-γTub (1:100; Sigma-Aldrich, T5326). Secondary antibodies conjugated to fluorescent dyes were obtained from Molecular Probes or Jackson ImmunoResearch, and they were used at a dilution of 1:200. Cell nuclei were stained with DAPI (Vector Laboratories) and F-actin with Alexa Fluor 633–conjugated phalloidin (Invitrogen).

Fluorescence images were recorded by using a Leica upright microscope DM-SL with Spectral Confocal acquisition software (Leica). Images were taken with an HCX Plan Apochromat 63×/1.32–0.6-NA oil confocal scanning objective. Fluorescent images for Fig. 1 (B–D, R, and S), Fig. 6 (E–G and O–R), and Fig. S4 were recorded by using an Inverted Leica laser-scanning spectral confocal microscope TCS SP2 (Leica). Images were taken with 20×/0.7-NA Imm/Corr (Fig. 1 B) or 63×/1.4-NA oil (inset in Fig. 1 B; Fig. 1, C, D, R, and S; and Fig. S4) scanning objectives. Fluorescent imaging was performed at 21°C. Details of fluorochromes used in individual experiments are described in the immunostaining procedures. The distance between focal planes in each Z-stack was 0.8 µm (unless otherwise stated). The micrographs in the figures represent single focal planes from confocal Z-stacks except Fig. 6 (E–G, I–K, and M–P) and Fig. 7 (G and H), which represent the sum of 2–4 (Fig. 6) or 10 (Fig. 7) focal planes from the Z-stack (the same number for the different genotypes in a given experiment) and that were generated with the Z project tool of the open source Fiji software. For image analysis, mutant and control specimens from the same experiment were processed in parallel. Samples were analyzed within the same work session when possible, using exactly the same acquisition parameters in the confocal microscope.

Embryos in Fig. S1 (D and E) were imaged on a Zeiss Axio Imager A1 microscope with a 40×/1.3-NA oil objective lens (Carl Zeiss) and with a CCD camera (AxioCam HRc; Carl Zeiss) controlled by AxioVision software (Carl Zeiss). All images were assembled using Adobe Photoshop CS3.

Antibody production
To generate an anti-Eph antibody, two rabbits were injected with the synthetic peptide containing amino acids 994–1,022 of the *Drosophila* Eph intracellular domain (LTTRPSPESDGN-HILDGQRGQNIFISTDLC, described in Scully et al., 1999). After three immunizations, the animals were bled, and the resulting sera were validated by immunofluorescence, immunohisto-chemistry, and in WBs (Fig. S1).

WBs
10 brains from third-instar larvae were dissected out in PBS, homogenized by repeated pipetting in fresh lysis buffer (50 mM Tris, pH 8.0, 150 mM NaCl, 0.1% SDS, 1 M EDTA, 1% Triton X-100, 1% sodium deoxycholate, protease inhibitors, 1 mM NaF, 100 mM Na$_3$VO$_4$, 2 mM PMSF, and Complete Protease Inhibitor Cocktail from Roche) and incubated on ice for 15 min. The protein extracts were centrifuged at 6,000 g at 4°C for 10 min and 5× Laemmli buffer with 0.1 M DTT was added to each sample, which was heated at 95°C for 10 min. After centrifugation at maximum speed (8,000 g) for 1 min, the protein extracts were resolved by SDS-PAGE. From the whole-protein extract, the material corresponding to five brains was loaded for Akt WBs (Fig. 6) or two brains for Eph WBs (Fig. S1). The Spectra Multicolor High Range Protein Ladder (Fermentas) was used as a molecular weight marker, and the PVDF filters were probed with the rabbit anti-pAkt (Ser473, 1:500; Cell Signaling Technology, 9271), rabbit anti-pan Akt (C67E7, 1:200; 4691), rabbit anti-Eph (1:3,000), mouse anti-α-tubulin (1:5,000; Sigma-Aldrich, T6199), or rabbit anti-Myc (1:5,000; Abcam, Ab9106), which were detected with appropriate HRP-coupled secondary antibodies.

EdU incorporation assays
Third-instar larval brains were dissected out in Shields and Sang M3 insect medium and incubated in fresh M3 medium containing 10% FBS and 40 µM EdU at RT for 1 h. The medium containing EdU was removed, and the brains were rinsed thrice with PBS. The brains were fixed with 4% PFA in in PBT (0.1% Triton X-100) at RT for 20 min and blocked with 0.1% BSA in PBT (0.3% Triton X-100). The Click-iT reaction was performed according to the manufacturer's instructions (Life Technology, C10640), and the slides were then immunostained for E-cadherin to label neuroepithelial cells and cyclin-E and mounted in Vectashield mounting medium.

Spindle angle measurement
Spindle angles were calculated using ImageJ, measuring the angle between a line linking both centrosomes and the planar apical surface. These measurements frequently required correction in the xy plane to allow both spindle poles to be present in a single Z-plane. To avoid overcorrection, only mitoses with centrosomes in the same or in two consecutive Z-planes were considered for quantification. The dataset was analyzed using a χ^2 test with Yates correction.

Mitotic cell distance measurement
The distance of the mitotic cell to the neuroepithelial apical surface was estimated by normalizing the distance from the metaphasic plate to the apical surface in relation to the total width of the NE (delimited by E-cadherin immunolabeling). At

least 52 mitoses from no fewer than six different brains were quantified for each experimental condition (see corresponding figures and figure legends for details).

Optic lobe area measurement

The optic lobe was defined by E-cadherin immunolabeling and measured using ImageJ. The Z-focal plane with the largest area was selected in each brain, and the data from the mutant was normalized with respect to the average of the control brains.

Estimation of the size of the NE

The size of the NE was estimated by measuring the depth of the corresponding confocal Z-stack. Each Z-stack (in micrometers) started from where the neuroepithelial cells appear and continued in an antero-posterior direction, terminating when the outer proliferation center (OPC) disappeared.

Cell death assays

Cleaved-Caspase (Dcp1) immunostaining was performed to measure cell death. E-cadherin was used to visualize the OPC NE, and only those Dcp1-positive cells within the OPC or in direct contact with it were counted. The values shown are the mean of the total number of Dcp1-positive cells per OPC.

Cell proliferation assays

EdU-positive cells in the NE were measured in frontal brain sections every 3 µm to ensure that the same cell was not counted twice. The area analyzed was defined by anatomical references, starting when neuroepithelial cells appear and following an antero-posterior direction, sampling five sections for each brain hemisphere. The final number of proliferating neuroepithelial cells was the mean number of EdU-positive neuroepithelial cells per hemisphere, and at least seven hemispheres from a minimum of four brains were analyzed for each experimental condition.

Quantification and statistical analysis

Band intensity was quantified in the WBs using Fiji software, and the experiments were repeated at least three times. A minimum of six brains were used in each experiment, and the cells labeled in the cell death and cell proliferation assays were counted by eye.

For statistical analysis, the data were first analyzed using the Shapiro–Wilk test to determine whether the sample followed a normal distribution. The data with a normal distribution were analyzed using the unpaired two-tailed Student's t test for two-sample comparison, after performing an F test for variances, or with one-way ANOVA (with Tukey's post hoc correction) for comparing three or more independent samples simultaneously. Data that did not follow a normal distribution were analyzed using a Mann–Whitney U test or a χ^2 proportion test in the case of the spindle angles (i.e., the proportion of populations with vertical divisions [>30°] were compared between the control and each of the mutant conditions). A Z test to compare two proportions was used in Fig. 7 T. The specific test used, the sample size (n), the SEM, or the SD of the population and the P value is indicated in each figure and/or figure legend; ****, $P \le 0.0001$; ***, $P \le 0.001$; **, $P \le 0.01$; and *, $P \le 0.05$.

Online supplemental material

Fig. S1 shows the specificity of the anti-Eph antibody both by immunofluorescence (in larval NE)/immunohistochemistry (in embryos) and by WB. Fig. S2 shows Eph^{KD} (kinase dead) and $Ephrin^{RNAi}$ mutant phenotypes affecting polarity cue local distribution and NE architecture similar to those observed in Eph^{x652}-null mutants. Fig. S3 shows how a constitutively activated form of aPKC is able to rescue the collapse in the subapical region observed in Eph^{x652}-null mutant neuroepithelia. Fig. S4 shows that both active myosin (Sqh^{EE}) and aPKC are required to suppress the Dlg1 apical expansion phenotype observed in Eph^{x652} dividing mutant cells.

References

Amano, M., M. Ito, K. Kimura, Y. Fukata, K. Chihara, T. Nakano, Y. Matsuura, and K. Kaibuchi. 1996. Phosphorylation and activation of myosin by Rho-associated kinase (Rho-kinase). *J. Biol. Chem.* 271:20246–20249. https://doi.org/10.1074/jbc.271.34.20246

Aoki, M., T. Yamashita, and M. Tohyama. 2004. EphA receptors direct the differentiation of mammalian neural precursor cells through a mitogen-activated protein kinase-dependent pathway. *J. Biol. Chem.* 279:32643–32650. https://doi.org/10.1074/jbc.M313247200

Arbeille, E., F. Reynaud, I. Sanyas, M. Bozon, K. Kindbeiter, F. Causeret, A. Pierani, J. Falk, F. Moret, and V. Castellani. 2015. Cerebrospinal fluid-derived Semaphorin3B orients neuroepithelial cell divisions in the apicobasal axis. *Nat. Commun.* 6:6366. https://doi.org/10.1038/ncomms7366

Arvanitis, D.N., A. Béhar, P. Tryoen-Tóth, J.O. Bush, T. Jungas, N. Vitale, and A. Davy. 2013. Ephrin B1 maintains apical adhesion of neural progenitors. *Development.* 140:2082–2092. https://doi.org/10.1242/dev.088203

Batlle, E., and D.G. Wilkinson. 2012. Molecular mechanisms of cell segregation and boundary formation in development and tumorigenesis. *Cold Spring Harb. Perspect. Biol.* 4:a008227. https://doi.org/10.1101/cshperspect.a008227

Bellaïche, Y., A. Radovic, D.F. Woods, C.D. Hough, M.L. Parmentier, C.J. O'Kane, P.J. Bryant, and F. Schweisguth. 2001. The Partner of Inscuteable/Discs-large complex is required to establish planar polarity during asymmetric cell division in Drosophila. *Cell.* 106:355–366. https://doi.org/10.1016/S0092-8674(01)00444-5

Bergstralh, D.T., T. Haack, and D. St Johnston. 2013a. Epithelial polarity and spindle orientation: intersecting pathways. *Philos. Trans. R. Soc. Lond. B Biol. Sci.* 368:20130291. https://doi.org/10.1098/rstb.2013.0291

Bergstralh, D.T., H.E. Lovegrove, and D. St Johnston. 2013b. Discs large links spindle orientation to apical-basal polarity in Drosophila epithelia. *Curr. Biol.* 23:1707–1712. https://doi.org/10.1016/j.cub.2013.07.017

Bergstralh, D.T., H.E. Lovegrove, and D. St Johnston. 2015. Lateral adhesion drives reintegration of misplaced cells into epithelial monolayers. *Nat. Cell Biol.* 17:1497–1503. https://doi.org/10.1038/ncb3248

Bergstralh, D.T., H.E. Lovegrove, I. Kujawiak, N.S. Dawney, J. Zhu, S. Cooper, R. Zhang, and D. St Johnston. 2016. Pins is not required for spindle orientation in the Drosophila wing disc. *Development.* 143:2573–2581. https://doi.org/10.1242/dev.135475

Bossing, T., and A.H. Brand. 2002. Dephrin, a transmembrane ephrin with a unique structure, prevents interneuronal axons from exiting the Drosophila embryonic CNS. *Development.* 129:4205–4218.

Bowman, S.K., R.A. Neumüller, M. Novatchkova, Q. Du, and J.A. Knoblich. 2006. The Drosophila NuMA Homolog Mud regulates spindle orientation in asymmetric cell division. *Dev. Cell.* 10:731–742. https://doi.org/10.1016/j.devcel.2006.05.005

Boyle, M., A. Nighorn, and J.B. Thomas. 2006. Drosophila Eph receptor guides specific axon branches of mushroom body neurons. *Development.* 133:1845–1854. https://doi.org/10.1242/dev.02353

Buttrick, G.J., and J.G. Wakefield. 2008. PI3-K and GSK-3: Akt-ing together with microtubules. *Cell Cycle.* 7:2621–2625. https://doi.org/10.4161/cc.7.17.6514

Buttrick, G.J., L.M. Beaumont, J. Leitch, C. Yau, J.R. Hughes, and J.G. Wakefield. 2008. Akt regulates centrosome migration and spindle orientation in the early Drosophila melanogaster embryo. *J. Cell Biol.* 180:537–548. https://doi.org/10.1083/jcb.200705085

Carminati, M., S. Gallini, L. Pirovano, A. Alfieri, S. Bisi, and M. Mapelli. 2016. Concomitant binding of Afadin to LGN and F-actin directs planar spindle orientation. *Nat. Struct. Mol. Biol.* 23:155–163. https://doi.org/10.1038/nsmb.3152

Castanon, I., and M. González-Gaitán. 2011. Oriented cell division in vertebrate embryogenesis. *Curr. Opin. Cell Biol.* 23:697–704. https://doi.org/10.1016/j.ceb.2011.09.009

Chang, Y.J., L. Zhou, R. Binari, A. Manoukian, T. Mak, H. McNeill, and V. Stambolic. 2016. The Rho Guanine Nucleotide Exchange Factor DRhoGEF2 Is a Genetic Modifier of the PI3K Pathway in Drosophila. *PLoS One.* 11:e0152259. https://doi.org/10.1371/journal.pone.0152259

Chong, L.D., E.K. Park, E. Latimer, R. Friesel, and I.O. Daar. 2000. Fibroblast growth factor receptor-mediated rescue of x-ephrin B1-induced cell dissociation in Xenopus embryos. *Mol. Cell. Biol.* 20:724–734. https://doi.org/10.1128/MCB.20.2.724-734.2000

Cramer, K.S., and I.J. Miko. 2016. Eph-ephrin signaling in nervous system development. *F1000 Res.* 5:413. https://doi.org/10.12688/f1000research.7417.1

den Elzen, N., C.V. Buttery, M.P. Maddugoda, G. Ren, and A.S. Yap. 2009. Cadherin adhesion receptors orient the mitotic spindle during symmetric cell division in mammalian epithelia. *Mol. Biol. Cell.* 20:3740–3750. https://doi.org/10.1091/mbc.e09-01-0023

di Pietro, F., A. Echard, and X. Morin. 2016. Regulation of mitotic spindle orientation: an integrated view. *EMBO Rep.* 17:1106–1130. https://doi.org/10.15252/embr.201642292

Durgan, J., N. Kaji, D. Jin, and A. Hall. 2011. Par6B and atypical PKC regulate mitotic spindle orientation during epithelial morphogenesis. *J. Biol. Chem.* 286:12461–12474. https://doi.org/10.1074/jbc.M110.174235

Furukawa, N., P. Ongusaha, W.J. Jahng, K. Araki, C.S. Choi, H.J. Kim, Y.H. Lee, K. Kaibuchi, B.B. Kahn, H. Masuzaki, et al. 2005. Role of Rho-kinase in regulation of insulin action and glucose homeostasis. *Cell Metab.* 2:119–129. https://doi.org/10.1016/j.cmet.2005.06.011

Gloerich, M., J.M. Bianchini, K.A. Siemers, D.J. Cohen, and W.J. Nelson. 2017. Cell division orientation is coupled to cell-cell adhesion by the E-cadherin/LGN complex. *Nat. Commun.* 8:13996. https://doi.org/10.1038/ncomms13996

Gong, Y., C. Mo, and S.E. Fraser. 2004. Planar cell polarity signalling controls cell division orientation during zebrafish gastrulation. *Nature.* 430:689–693. https://doi.org/10.1038/nature02796

Goulding, M.B., J.C. Canman, E.N. Senning, A.H. Marcus, and B. Bowerman. 2007. Control of nuclear centration in the C. elegans zygote by receptor-independent Galpha signaling and myosin II. *J. Cell Biol.* 178:1177–1191. https://doi.org/10.1083/jcb.200703159

Guilgur, L.G., P. Prudêncio, T. Ferreira, A.R. Pimenta-Marques, and R.G. Martinho. 2012. Drosophila aPKC is required for mitotic spindle orientation during symmetric division of epithelial cells. *Development.* 139:503–513. https://doi.org/10.1242/dev.071027

Hao, Y., Q. Du, X. Chen, Z. Zheng, J.L. Balsbaugh, S. Maitra, J. Shabanowitz, D.F. Hunt, and I.G. Macara. 2010. Par3 controls epithelial spindle orientation by aPKC-mediated phosphorylation of apical Pins. *Curr. Biol.* 20:1809–1818. https://doi.org/10.1016/j.cub.2010.09.032

Hertwig, O. 1884. Das Problem der Befruchtung und der Isotropie des Eies, eine Theory der Vererbung. *Jenaische Zeitschrift fuer Naturwissenschaft.* 18:21–23.

Hopkins, B.D., C. Hodakoski, D. Barrows, S.M. Mense, and R.E. Parsons. 2014. PTEN function: the long and the short of it. *Trends Biochem. Sci.* 39:183–190. https://doi.org/10.1016/j.tibs.2014.02.006

Izumi, Y., N. Ohta, K. Hisata, T. Raabe, and F. Matsuzaki. 2006. Drosophila Pins-binding protein Mud regulates spindle-polarity coupling and centrosome organization. *Nat. Cell Biol.* 8:586–593. https://doi.org/10.1038/ncb1409

Johnston, C.A., K. Hirono, K.E. Prehoda, and C.Q. Doe. 2009. Identification of an Aurora-A/PinsLINKER/Dlg spindle orientation pathway using induced cell polarity in S2 cells. *Cell.* 138:1150–1163. https://doi.org/10.1016/j.cell.2009.07.041

Johnston, C.A., L. Manning, M.S. Lu, O. Golub, C.Q. Doe, and K.E. Prehoda. 2013. Formin-mediated actin polymerization cooperates with Mushroom body defect (Mud)-Dynein during Frizzled-Dishevelled spindle orientation. *J. Cell Sci.* 126:4436–4444. https://doi.org/10.1242/jcs.129544

Jones, T.L., L.D. Chong, J. Kim, R.H. Xu, H.F. Kung, and I.O. Daar. 1998. Loss of cell adhesion in Xenopus laevis embryos mediated by the cytoplasmic domain of XLerk, an erythropoietin-producing hepatocellular ligand. *Proc. Natl. Acad. Sci. USA.* 95:576–581. https://doi.org/10.1073/pnas.95.2.576

Jordan, P., and R. Karess. 1997. Myosin light chain-activating phosphorylation sites are required for oogenesis in Drosophila. *J. Cell Biol.* 139:1805–1819. https://doi.org/10.1083/jcb.139.7.1805

Jungas, T., R.T. Perchey, M. Fawal, C. Callot, C. Froment, O. Burlet-Schiltz, A. Besson, and A. Davy. 2016. Eph-mediated tyrosine phosphorylation of citron kinase controls abscission. *J. Cell Biol.* 214:555–569. https://doi.org/10.1083/jcb.201602057

Kania, A., and R. Klein. 2016. Mechanisms of ephrin-Eph signalling in development, physiology and disease. *Nat. Rev. Mol. Cell Biol.* 17:240–256. https://doi.org/10.1038/nrm.2015.16

Keder, A., N. Rives-Quinto, B.L. Aerne, M. Franco, N. Tapon, and A. Carmena. 2015. The hippo pathway core cassette regulates asymmetric cell division. *Curr. Biol.* 25:2739–2750. https://doi.org/10.1016/j.cub.2015.08.064

Kishikawa, M., A. Suzuki, and S. Ohno. 2008. aPKC enables development of zonula adherens by antagonizing centripetal contraction of the circumferential actomyosin cables. *J. Cell Sci.* 121:2481–2492. https://doi.org/10.1242/jcs.024109

Kosodo, Y. 2012. Interkinetic nuclear migration: beyond a hallmark of neurogenesis. *Cell. Mol. Life Sci.* 69:2727–2738. https://doi.org/10.1007/s00018-012-0952-2

Lancaster, O.M., and B. Baum. 2014. Shaping up to divide: coordinating actin and microtubule cytoskeletal remodelling during mitosis. *Semin. Cell Dev. Biol.* 34:109–115. https://doi.org/10.1016/j.semcdb.2014.02.015

Laussu, J., A. Khuong, J. Gautrais, and A. Davy. 2014. Beyond boundaries--Eph:ephrin signaling in neurogenesis. *Cell Adhes. Migr.* 8:349–359. https://doi.org/10.4161/19336918.2014.969990

Lawlor, M.A., and D.R. Alessi. 2001. PKB/Akt: a key mediator of cell proliferation, survival and insulin responses? *J. Cell Sci.* 114:2903–2910.

Lee, H.S., and I.O. Daar. 2009. EphrinB reverse signaling in cell-cell adhesion: is it just par for the course? *Cell Adhes. Migr.* 3:250–255. https://doi.org/10.4161/cam.3.3.8211

Lee, H.S., T.G. Nishanian, K. Mood, Y.S. Bong, and I.O. Daar. 2008. EphrinB1 controls cell-cell junctions through the Par polarity complex. *Nat. Cell Biol.* 10:979–986. https://doi.org/10.1038/ncb1758

Li, Z., X. Dong, Z. Wang, W. Liu, N. Deng, Y. Ding, L. Tang, T. Hla, R. Zeng, L. Li, and D. Wu. 2005. Regulation of PTEN by Rho small GTPases. *Nat. Cell Biol.* 7:399–404. https://doi.org/10.1038/ncb1236

Lisabeth, E.M., G. Falivelli, and E.B. Pasquale. 2013. Eph receptor signaling and ephrins. *Cold Spring Harb. Perspect. Biol.* 5:a009159. https://doi.org/10.1101/cshperspect.a009159

Lu, M.S., and C.A. Johnston. 2013. Molecular pathways regulating mitotic spindle orientation in animal cells. *Development.* 140:1843–1856. https://doi.org/10.1242/dev.087627

Luo, J., B.D. Manning, and L.C. Cantley. 2003. Targeting the PI3K-Akt pathway in human cancer: rationale and promise. *Cancer Cell.* 4:257–262. https://doi.org/10.1016/S1535-6108(03)00248-4

Luxenburg, C., H.A. Pasolli, S.E. Williams, and E. Fuchs. 2011. Developmental roles for Srf, cortical cytoskeleton and cell shape in epidermal spindle orientation. *Nat. Cell Biol.* 13:203–214. https://doi.org/10.1038/ncb2163

McCaffrey, L.M., and I.G. Macara. 2011. Epithelial organization, cell polarity and tumorigenesis. *Trends Cell Biol.* 21:727–735. https://doi.org/10.1016/j.tcb.2011.06.005

Miller, K.G., C.M. Field, and B.M. Alberts. 1989. Actin-binding proteins from Drosophila embryos: a complex network of interacting proteins detected by F-actin affinity chromatography. *J. Cell Biol.* 109:2963–2975. https://doi.org/10.1083/jcb.109.6.2963

Morin, X., and Y. Bellaïche. 2011. Mitotic spindle orientation in asymmetric and symmetric cell divisions during animal development. *Dev. Cell.* 21: 102–119. https://doi.org/10.1016/j.devcel.2011.06.012

Nakajima, Y., E.J. Meyer, A. Kroesen, S.A. McKinney, and M.C. Gibson. 2013. Epithelial junctions maintain tissue architecture by directing planar spindle orientation. *Nature.* 500:359–362. https://doi.org/10.1038/nature12335

Nestor-Bergmann, A., G. Goddard, and S. Woolner. 2014. Force and the spindle: mechanical cues in mitotic spindle orientation. *Semin. Cell Dev. Biol.* 34:133–139. https://doi.org/10.1016/j.semcdb.2014.07.008

Noren, N.K., and E.B. Pasquale. 2004. Eph receptor-ephrin bidirectional signals that target Ras and Rho proteins. *Cell. Signal.* 16:655–666. https://doi.org/10.1016/j.cellsig.2003.10.006

North, H.A., X. Zhao, S.M. Kolk, M.A. Clifford, D.M. Ziskind, and M.J. Donoghue. 2009. Promotion of proliferation in the developing cerebral cortex by EphA4 forward signaling. *Development.* 136:2467–2476. https://doi.org/10.1242/dev.034405

Pease, J.C., and J.S. Tirnauer. 2011. Mitotic spindle misorientation in cancer--out of alignment and into the fire. *J. Cell Sci.* 124:1007–1016. https://doi.org/10.1242/jcs.081406

Qiu, R., X. Wang, A. Davy, C. Wu, K. Murai, H. Zhang, J.G. Flanagan, P. Soriano, and Q. Lu. 2008. Regulation of neural progenitor cell state by ephrin-B. *J. Cell Biol.* 181:973–983. https://doi.org/10.1083/jcb.200708091

Rakotomamonjy, J., M. Brunner, C. Jüschke, K. Zang, E.J. Huang, L.F. Reichardt, and A. Chenn. 2017. Afadin controls cell polarization and mitotic spindle orientation in developing cortical radial glia. *Neural Dev.* 12:7. https://doi.org/10.1186/s13064-017-0085-2

Rives-Quinto, N., M. Franco, A. de Torres-Jurado, and A. Carmena. 2017. Synergism between *canoe* and *scribble* mutations causes tumor-like overgrowth via Ras activation in neural stem cells and epithelia. *Development.* 144:2570–2583. https://doi.org/10.1242/dev.148171

Rujano, M.A., L. Sanchez-Pulido, C. Pennetier, G. le Dez, and R. Basto. 2013. The microcephaly protein Asp regulates neuroepithelium morphogenesis by controlling the spatial distribution of myosin II. *Nat. Cell Biol.* 15: 1294–1306. https://doi.org/10.1038/ncb2858

Saburi, S., I. Hester, E. Fischer, M. Pontoglio, V. Eremina, M. Gessler, S.E. Quaggin, R. Harrison, R. Mount, and H. McNeill. 2008. Loss of Fat4 disrupts PCP signaling and oriented cell division and leads to cystic kidney disease. *Nat. Genet.* 40:1010–1015. https://doi.org/10.1038/ng.179

Scheid, M.P., and J.R. Woodgett. 2001. PKB/AKT: functional insights from genetic models. *Nat. Rev. Mol. Cell Biol.* 2:760–768. https://doi.org/10.1038/35096067

Scully, A.L., M. McKeown, and J.B. Thomas. 1999. Isolation and characterization of Dek, a Drosophila eph receptor protein tyrosine kinase. *Mol. Cell. Neurosci.* 13:337–347. https://doi.org/10.1006/mcne.1999.0752

Ségalen, M., C.A. Johnston, C.A. Martin, J.G. Dumortier, K.E. Prehoda, N.B. David, C.Q. Doe, and Y. Bellaïche. 2010. The Fz-Dsh planar cell polarity pathway induces oriented cell division via Mud/NuMA in Drosophila and zebrafish. *Dev. Cell.* 19:740–752. https://doi.org/10.1016/j.devcel.2010.10.004

Severson, A.F., and B. Bowerman. 2003. Myosin and the PAR proteins polarize microfilament-dependent forces that shape and position mitotic spindles in Caenorhabditis elegans. *J. Cell Biol.* 161:21–26. https://doi.org/10.1083/jcb.200210171

Shamah, S.M., M.Z. Lin, J.L. Goldberg, S. Estrach, M. Sahin, L. Hu, M. Bazalakova, R.L. Neve, G. Corfas, A. Debant, and M.E. Greenberg. 2001. EphA receptors regulate growth cone dynamics through the novel guanine nucleotide exchange factor ephexin. *Cell.* 105:233–244. https://doi.org/10.1016/S0092-8674(01)00314-2

Siller, K.H., C. Cabernard, and C.Q. Doe. 2006. The NuMA-related Mud protein binds Pins and regulates spindle orientation in Drosophila neuroblasts. *Nat. Cell Biol.* 8:594–600. https://doi.org/10.1038/ncb1412

Sordella, R., W. Jiang, G.C. Chen, M. Curto, and J. Settleman. 2003. Modulation of Rho GTPase signaling regulates a switch between adipogenesis and myogenesis. *Cell.* 113:147–158. https://doi.org/10.1016/S0092-8674(03)00271-X

Speicher, S., A. Fischer, J. Knoblich, and A. Carmena. 2008. The PDZ protein Canoe regulates the asymmetric division of Drosophila neuroblasts and muscle progenitors. *Curr. Biol.* 18:831–837. https://doi.org/10.1016/j.cub.2008.04.072

Tang, N., W.F. Marshall, M. McMahon, R.J. Metzger, and G.R. Martin. 2011. Control of mitotic spindle angle by the RAS-regulated ERK1/2 pathway determines lung tube shape. *Science.* 333:342–345. https://doi.org/10.1126/science.1204831

Wahl, S., H. Barth, T. Ciossek, K. Aktories, and B.K. Mueller. 2000. Ephrin-A5 induces collapse of growth cones by activating Rho and Rho kinase. *J. Cell Biol.* 149:263–270. https://doi.org/10.1083/jcb.149.2.263

Wang, Y., and V. Riechmann. 2007. The role of the actomyosin cytoskeleton in coordination of tissue growth during Drosophila oogenesis. *Curr. Biol.* 17:1349–1355. https://doi.org/10.1016/j.cub.2007.06.067

Wee, B., C.A. Johnston, K.E. Prehoda, and C.Q. Doe. 2011. Canoe binds RanGTP to promote Pins(TPR)/Mud-mediated spindle orientation. *J. Cell Biol.* 195:369–376. https://doi.org/10.1083/jcb.201102130

Werts, A.D., and B. Goldstein. 2011. How signaling between cells can orient a mitotic spindle. *Semin. Cell Dev. Biol.* 22:842–849. https://doi.org/10.1016/j.semcdb.2011.07.011

Wilkinson, D.G. 2014. Regulation of cell differentiation by Eph receptor and ephrin signaling. *Cell Adhes. Migr.* 8:339–348. https://doi.org/10.4161/19336918.2014.970007

Williams, S.E., and E. Fuchs. 2013. Oriented divisions, fate decisions. *Curr. Opin. Cell Biol.* 25:749–758. https://doi.org/10.1016/j.ceb.2013.08.003

Winter, C.G., B. Wang, A. Ballew, A. Royou, R. Karess, J.D. Axelrod, and L. Luo. 2001. Drosophila Rho-associated kinase (Drok) links Frizzled-mediated planar cell polarity signaling to the actin cytoskeleton. *Cell.* 105:81–91. https://doi.org/10.1016/S0092-8674(01)00298-7

Xia, J., J.M. Swiercz, I. Bañón-Rodríguez, I. Matković, G. Federico, T. Sun, T. Franz, C.H. Brakebusch, A. Kumanogoh, R.H. Friedel, et al. 2015. Semaphorin-Plexin Signaling Controls Mitotic Spindle Orientation during Epithelial Morphogenesis and Repair. *Dev. Cell.* 33:299–313. https://doi.org/10.1016/j.devcel.2015.02.001

Yu, F., X. Morin, Y. Cai, X. Yang, and W. Chia. 2000. Analysis of partner of inscuteable, a novel player of Drosophila asymmetric divisions, reveals two distinct steps in inscuteable apical localization. *Cell.* 100:399–409. https://doi.org/10.1016/S0092-8674(00)80676-5

Zheng, Z., Q. Wan, J. Liu, H. Zhu, X. Chu, and Q. Du. 2013. Evidence for dynein and astral microtubule-mediated cortical release and transport of Gαi/LGN/NuMA complex in mitotic cells. *Mol. Biol. Cell.* 24:901–913. https://doi.org/10.1091/mbc.e12-06-0458

Žigman, M., A. Trinh, S.E. Fraser, and C.B. Moens. 2011. Zebrafish neural tube morphogenesis requires Scribble-dependent oriented cell divisions. *Curr. Biol.* 21:79–86. https://doi.org/10.1016/j.cub.2010.12.005